The Influence of Potential Evaporation on the Variabilities of Simulated Soil Wetness and Climate

THOMAS L. DELWORTH AND SYUKURO MANABE

Geophysical Fluid Dynamics Laboratory/NOAA, Princeton University, Princeton, New Jersey

(Manuscript received 20 November 1987, in final form 10 February 1988)

ABSTRACT

An atmospheric general circulation model with prescribed sea surface temperature and cloudiness was integrated for 50 years in order to study atmosphere–land surface interactions. The temporal variability of model soil moisture and precipitation have been studied in an effort to understand the interactions of these variables with other components of the climate system.

Temporal variability analysis has shown that the spectra of monthly mean precipitation over land are close to white at all latitudes, with total variance decreasing poleward. In contrast, the spectra of soil moisture are red, and become more red with increasing latitude. As a measure of this redness, half of the total variance of a composite tropical soil moisture spectrum occurs at periods longer than nine months, while at high latitudes, half of the total variance of a composite soil moisture spectrum occurs at periods longer than 22 months. The spectra of soil moisture also exhibit marked longitudinal variations.

These spectral results may be viewed in the light of stochastic theory. The formulation of the GFDL soil moisture parameterization is mathematically similar to a stochastic process. According to this model, forcing of a system by an input white noise variable (precipitation) will yield an output variable (soil moisture) with a red spectrum, the redness of which is controlled by a damping term (potential evaporation). Thus, the increasingly red nature of the soil moisture spectra at higher latitudes is a result of declining potential evaporation values at higher latitudes. Physically, soil moisture excesses are dissipated more slowly at high latitudes where the energy available for evaporation is small.

Some of the longitudinal variations in soil moisture spectra result from longitudinal variations in potential evaporation, while others are explicable in terms of the value of the ratio of potential evaporation to precipitation. Regions where this value is less than one are characaterized by frequent runoff and short time scales of soil moisture variability. By preventing excessive positive anomalies of soil moisture, the runoff process hastens the return of soil moisture values to their mean state, thereby shortening soil moisture time scales.

Through the use of a second GCM integration with prescribed soil moisture, it was shown that interactive soil moisture may substantially increase summer surface air temperature variability. Soil moisture interacts with the atmosphere primarily through the surface energy balance. The degree of soil saturation strongly influences the partitioning of outgoing energy from the surface between the latent and sensible heat fluxes. Interactive soil moisture allows larger variations of these fluxes, thereby increasing the variance of surface air temperature. Because the flux of latent heat is directly proportional to potential evaporation under conditions of sufficient moisture, the influence of soil moisture on the atmosphere is greatest when the potential evaporation value is large. This occurs most frequently in the tropics and summer hemisphere extratropics.

1. Introduction

The low frequency nature of soil wetness variability has been recognized for some time. Namias (1958, 1963), in studies of persistence of atmospheric circulation, noted that seasonal anomalies of soil wetness could have an impact on the seasonal cycle of the atmosphere. Subsequent studies of soil wetness, frequently utilizing general circulation models (GCMs), have examined the interactions between persistent anomalous soil wetness conditions and the atmosphere.

Shukla and Mintz (1982) have shown the tremendous influence that persistent anomalies of soil wetness have on the climate of a GCM, especially in the tropics and summer hemisphere extratropics. The most pronounced effects are on surface air temperature, surface pressure and precipitation. They also reported that time varying soil wetness has an influence on the annual cycle of the atmosphere. "In the extratropics, with its large seasonal changes, the soil plays a role analogous to that of the ocean. The ocean stores some of the radiational energy it receives in summer and uses it to heat the atmosphere over the ocean in winter. The soil stores some of the precipitation it receives in winter and uses it to humidify the atmosphere in summer."

Walker and Rowntree (1977) and Rowntree and Bolton (1983) performed model studies over Africa and Europe respectively. Their results demonstrated not only the time mean effect of persistent soil wetness anomalies on the atmosphere, but also showed that the

Corresponding author address: Thomas Delworth, GFDL/NOAA, Princeton University, Princeton, NJ 08542.

atmosphere may respond to these anomalies in such a way as to perpetuate the initial soil wetness anomalies. The time scale for such persistence appears to be at least on the order of weeks.

Rind (1982) examined the importance of soil wetness anomalies for summertime model predictability over North America. Given an early summer anomaly of soil wetness over the entire United States, he found the subsequent summer model conditions to be statistically different from a control run. He concluded that ". . . a knowledge of the ground moisture at the beginning of summer might allow for improved summer temperature forecasts. . . ."

Yeh et al. (1984), using a model with idealized geography, also discussed the atmospheric response to initially prescribed soil wetness anomalies. In addition to describing a feedback process that may have helped to prolong the initial soil wetness anomalies, they noted that the persistence of soil wetness anomalies depends significantly upon the latitude.

Gordon and Hunt (1987) were among the first to explicitly study the variability of soil moisture computed in an atmospheric model. Their results illustrate some of the scales of variability inherent in model-computed soil moisture. In particular, they found that in their model with a prescribed seasonal cycle of sea surface temperatures, droughts occurred on an interannual time scale.

While most of these studies have focused on the atmospheric effects of initially prescribed soil wetness anomalies and their ability to sustain themselves through feedback processes, our work explicitly studies the temporal variability of model computed interactive soil wetness, and attempts to identify the physical mechanisms controlling the time scales of that variability. We also examine the contributions that soil wetness temporal variability makes to model-computed atmospheric variability in the form of summer surface air temperatures. Our approach is to analyze the output from two long term GCM integrations (one with, and another without land surface-atmosphere interactions) in order to identify the relevant physical mechanisms. The lengths of these two integrations are 50 and 25 years, respectively. Although the soil wetness parameterization employed in the GCM is very simple, we feel that it includes the fundamental hydrological mechanisms of importance, and is thus adequate to identify the physical mechanisms controlling soil wetness temporal variability. In addition, its very simplicity enables a clearer identification and understanding of those mechanisms. We have also used a zero-dimensional model to more explicitly investigate the mechanisms of soil wetness temporal variability. The temporal variability characteristics of another GCM soil wetness parameterization are discussed in appendix B in order to assess the generality of our results.

Some of the framework for our study is derived from the work of Hasselmann (1976) and Frankignoul and Hasselmann (1977). Their work has shown that ". . . large-scale, long-time sea surface temperature anomalies may be explained naturally as the response of the oceanic surface layer to short time-scale atmospheric forcing. The white-noise spectrum of the atmospheric input produces a red response spectrum, with most of the variance concentrated in very long periods." The ocean surface layer acts as an integrator of the white noise atmospheric forcing. The sea surface temperature anomalies are in turn damped by fluxes of latent heat, sensible heat and radiation. This process may be approximated by a first-order Markov model.

We shall attempt to make the analogy that anomalies in soil moisture are the response of the soil layer to short time-scale rainfall forcing. We shall show that the white-noise spectrum of the rainfall plus snowmelt input produces a red response spectrum of soil moisture, with most of the variance concentrated in very long periods. The soil acts as an integrator of the white-noise rainfall plus snowmelt forcing. Soil moisture anomalies are in turn damped by evaporation. GCM-computed soil wetness temporal variability may thus be viewed as a first-order Markov process (red noise), forced by rainfall plus snowmelt and damped by evaporation. The spectral properties of this red-noise process may then be related to the geographically varying climatic parameters of potential evaporation and rainfall.

It is important to understand the mechanisms of low frequency soil wetness variability because of the aforementioned impact of soil wetness anomalies on climate. The primary effect of soil wetness anomalies is on the surface heat balance. The outgoing surface heat flux is partitioned into latent and sensible heat fluxes. Anomalous soil wetness conditions change this partitioning, and can have a substantial influence on low level atmospheric temperature and moisture content. These soil wetness anomalies, if of sufficient magnitude, duration, and spatial coherence, can have major impacts on climate and climatic variability. An understanding of low frequency soil wetness variability may lead to a better knowledge of low frequency atmospheric variability.

2. Model

a. Model structure

The model used is similar to models used in previous GFDL climate studies, with the exception of the computation of the atmospheric moisture field. This procedure will be discussed later. A further description of the other components of the model may be found in Manabe and Hahn (1981), or Manabe et al. (1979). The version of the model employed for this study consists of two parts: (i) a general circulation model of the atmosphere, and (ii) a heat and water balance over the continents. Seasonally varying sea ice and sea surface temperature fields are prescribed at all ocean grid points based on observed monthly mean fields.

The atmospheric general circulation model is very similar to that described by Manabe and Hahn (1981). The spectral computations employed the "rhomboidal 15" wavenumber truncation, in which 15 associated Legendre functions are retained for each of 15 Fourier components with the lowest zonal wavenumbers. Vertical derivatives appearing in the prognostic equations are computed by a centered, second-order finite difference with nine unevenly spaced levels.

The spectrally truncated representation of any field contains errors relative to the true field. These errors are amplified for fields, such as atmospheric moisture, which have small spatial scales. The spectral truncation of the field of atmospheric moisture often results in fictitious supersaturation and negative mixing ratios of water vapor. Because of these difficulties, a finite difference scheme was employed for atmospheric moisture, the details of which are discussed in appendix A. It was found that utilization of the finite difference scheme substantially mitigated the aforementioned difficulties.

Precipitation is predicted whenever supersaturation occurs in the model. This supersaturation can be the result of either large scale condensation or convective adjustment (see Manabe et al. 1965 for details of the convective adjustment scheme). If precipitation occurs while the air temperature just above the surface is below freezing, snowfall is forecast; otherwise, any precipitation is assumed to fall as rain.

The distribution of incoming solar radiation at the top of the atmosphere is prescribed; the diurnal cycle is omitted. The mixing ratio of carbon dioxide is assumed to be constant everywhere, whereas ozone is specified as a function of latitude, height and season. Cloud cover is prescribed to be zonally uniform and invariant with respect to season.

Over the continents surface temperature is determined such that no heat is stored in the soil. A balance is achieved among net incoming solar radiation, net outgoing longwave radiation, the sensible heat flux and the latent heat flux. The partitioning of energy among these components is controlled by soil wetness and low level atmospheric variables.

A snow budget is computed at the surface in which a change of snow depth is predicted as the net contributions from snowfall, sublimation, and snowmelt, with the latter two determined from the surface heat budget. Further details of the prognostic system of water vapor are found in Manabe et al. (1965).

The groundwater budget is computed by the "bucket method." The soil is assumed to have a water-holding capacity of 15 cm. If the computed soil moisture exceeds this amount, the excess is assumed to run off. Changes in soil moisture are computed from the rates of rainfall, evaporation, snowmelt, and runoff. Evaporation from the soil is determined as a function of soil wetness and the potential evaporation rate. Specifically, the parameterization is

$$\frac{dw(t)}{dt} = -E_p f\left(\frac{w(t)}{w_{FC}}\right) + \text{rainfall} + \text{snowmelt} - \text{runoff} \tag{1}$$

where

$w(t)$ soil moisture (cm)
w_{FC} field capacity (=15 cm)
E_p potential evaporation (cm d^{-1})

$$E_p = -\rho C_D |V_9| [q_9 - q_s(T_*)] \tag{2}$$

where

ρ the density of the air (g cm^{-3})
C_D the drag coefficient
V_9 the wind speed at the lowest model level
q_9 the mixing ratio at the lowest model level
$q_s(T_*)$ the saturation mixing ratio for the ground surface temperature
T_* the ground surface temperature

$$f\left(\frac{w(t)}{w_{FC}}\right) = \begin{cases} \left(\dfrac{w(t)}{0.75 w_{FC}}\right) & \text{if } w < 0.75 w_{FC} \\ 1 & \text{if } w > 0.75 w_{FC} \end{cases} . \tag{3}$$

From an isothermal atmosphere at rest the model was integrated for several years to reach a state of statistical equilibrium within the context of a seasonal model. From that point, a 50-year integration was performed. Analysis of the output of that 50-year run was performed on monthly mean data unless otherwise noted.

b. *Simulation capability*

To develop an appreciation of the model's ability to simulate the large scale features of hydrology, the model computed and observed Northern Hemisphere winter and summer mean maps of precipitation are presented in Figs. 1 and 2 respectively. For the Northern Hemisphere winter, continental precipitation is somewhat excessive over central and northern North America and southern Asia, while in fair agreement with observations elsewhere. The intertropical convergence zone (ITCZ) is not as sharply defined as in the observations, particularly over the eastern Pacific. The simulation is not as accurate for the Northern Hemisphere summer. Model precipitation exceeds observed values over the Arctic, northeastern Siberia and southeastern Africa. The Indian monsoon is not well simulated. Most of the Indian subcontinent is too wet, while the maximum in the observed precipitation data to the north of the Bay of Bengal is too intense in the model data. The ITCZ in Africa is too broad, extending into what should be the Saharan desert.

Model computed fields of summer and winter mean soil moisture are shown in Fig. 3. The soil moisture values are expressed as a fraction of field capacity (sat-

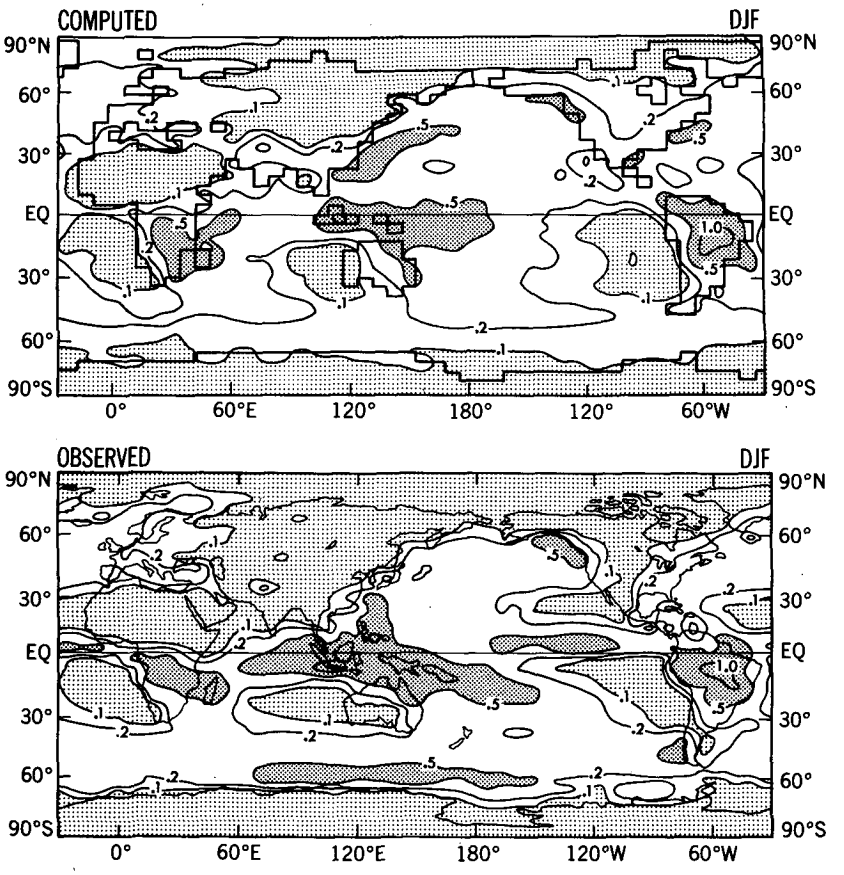

FIG. 1. Mean precipitation rates for December–February. Units are cm d^{-1}. Densely stippled areas represent precipitation rates greater than 0.5 cm d^{-1}, while lightly stippled areas represent precipitation rates of less than 0.1 cm d^{-1}. Both maps are smoothed. (Top) Model computed (smoothed with a nine point filter) and (bottom) observed, from Jaeger (1976).

uration) to more readily permit comparison to schemes with different field capacities. It is somewhat difficult to assess the simulation of the large scale distribution of soil wetness when this field has not been observed in nature. However, we can examine whether the patterns of computed soil moisture values are consistent with our perception of the global distribution of wetness at continental surfaces.

For the Northern Hemisphere summer, the soil wetness simulation is reasonable at most locations. The problems discussed earlier in connection with the simulation of the precipitation fields are also present in the soil wetness simulations. In particular, the moist zone in central Africa extends too far north in the summer, as does the Asian monsoon region. Over North and South America the computed soil wetness appears to be in at least qualitative agreement with observed precipitation.

The soil tends to be wetter in the Northern Hemisphere winter than in summer, and is nearly saturated over Europe, the eastern portion of Eurasia and most of North America. In both winter and summer seasons, the simulated values of soil moisture are low over most of the arid regions of the world, i.e., the Sahara, Gobi, Kalahari and Patagonian deserts, as well as most of Australia.

The annual mean values of runoff, both model-computed and observed, are shown in Fig. 4. There is good agreement globally between the two fields. The observed maxima over southeast Asia and northern South America are reproduced in the model, as are the minima over northern Africa, central Asia, Australia and southwestern North America. There appears to be an excess of runoff relative to the observations in the region immediately to the east of the Himalayas.

3. Spectral results

We first use spectral analysis to describe the temporal variability of model computed soil moisture. Anomaly time series of monthly mean soil moisture were computed at each grid point by subtracting the appropriate ensemble monthly mean soil moisture values from the individual monthly mean soil moisture values. The same procedure was performed for precipitation, defined as rainfall plus snowfall (hereafter denoted by

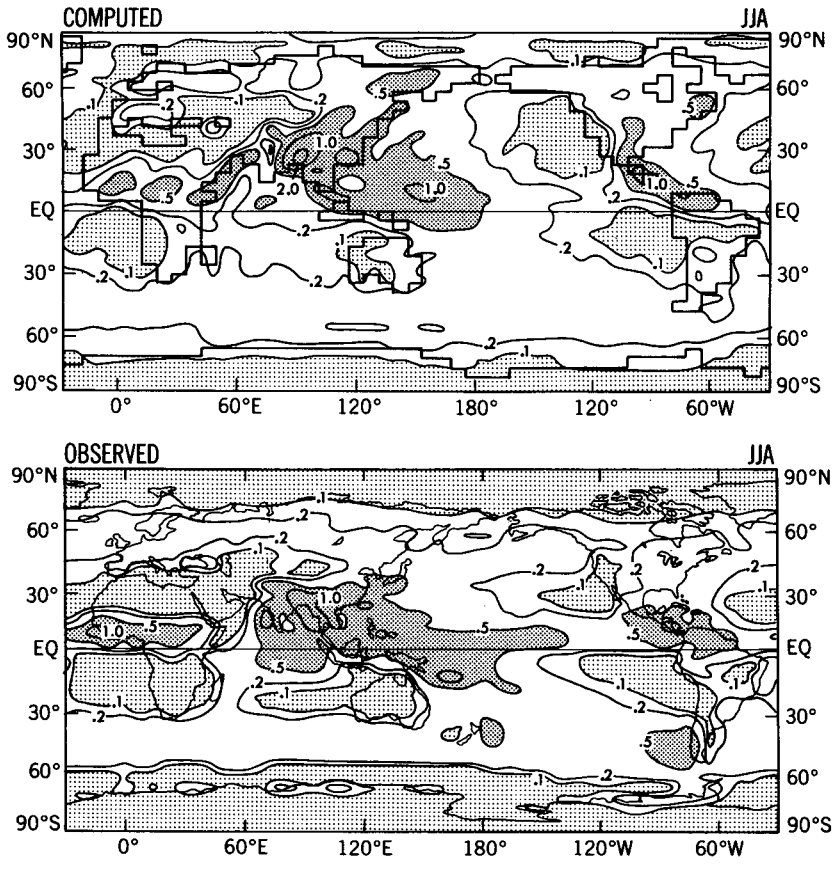

FIG. 2. As in Fig. 1 but for June–August.

RSNF) as well as for the time series of rainfall plus snowmelt (hereafter denoted by RSNM). This RSNM time series may be viewed as the actual forcing term of the soil wetness parameterization, as seen in (1). Spectral analysis was performed on these time series at each grid point. The spectra were normalized by their respective total variances, thereby allowing spectra from different regions to be composited without the spectra from regions of high variance overwhelming the spectra from regions of low variance. The soil moisture, RSNF and RSNM spectra were then zonally averaged over all land points. Based on similarities of spectral shape, mean precipitation values, and soil moisture values, the Northern Hemisphere zonally averaged spectra were further composited into four broad bands defined in Table 1. These band averaged spectra, representative of the large scale latitudinal variations of spectral shape, are shown in Fig. 5.

The most basic feature of the soil moisture spectra is their resemblance to red noise. In contrast, the RSNF and RSNM spectra bear a resemblance to white noise. Further, the "redness" of the soil moisture spectra increases with latitude, while there is little variation with latitude in the RSNF or RSNM spectra (although there is a slight suggestion of redder spectra in the subtropical and midlatitude bands). One interesting point in the high latitude spectra is the difference between the RSNF and the RSNM spectra. Because snowmelt is concentrated in a two to three month period in the spring, the RSNM spectrum possesses relatively more variance at higher frequencies than the RSNF spectrum.

A very prominent feature is the long time scale associated with all the soil moisture spectra. Large amounts of variance are located at periods of one year or more, suggesting that soil moisture may play a role in low frequency atmospheric variability. With this possibility, it is desirable to understand the mechanisms by which this low frequency soil moisture variability is generated and to assess its contribution to the overall climatic spectrum.

4. Stochastic model theory

Based on the spectra discussed in the previous section, one might speculate that the temporal variability of soil moisture may be governed by a process similar to red noise. Such an argument will be made in this section. In order to do so, a brief review of the basic formulations of a red noise process is needed. These ideas may then be used to interpret the GCM results.

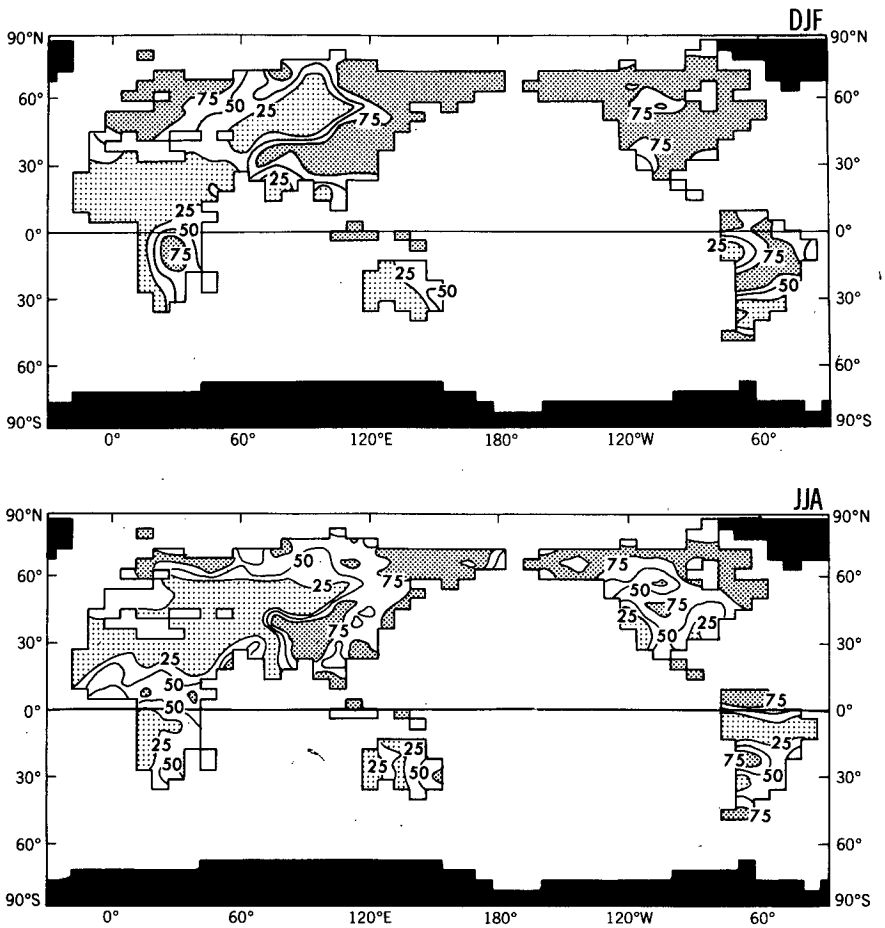

FIG. 3. Model-computed soil wetness fields. Units are percent saturation. Densely stippled areas represent saturation values greater than 75%, while lightly stippled areas represent saturation values less than 25%. Solid black regions are permanently ice covered. (Top) December–February (DJF) average and (bottom) June–August (JJA) average.

What is commonly called "red noise" in meteorology is the output of a first-order Markov process. This process is defined by

$$\frac{dy(t)}{dt} = -\lambda y(t) + z(t) \tag{4}$$

where λ is a constant and $z(t)$ is a white noise process.

Physically, this represents a system possessing an inherent exponential damping, but which is continually forced by some random (white noise) process. It is important to note that the characteristic time scale of the input time series is much shorter than the characteristic time scale of the response (Hasselmann 1976). The spectral response of such a system is given by

$$G(\omega) = \frac{F}{\omega^2 + \lambda^2} \tag{5}$$

where

$G(\omega)$ the spectral response
F the amplitude of the spectrum of the white noise forcing
ω the angular frequency
λ the constant from (4).

One can see that (5) lends itself mathematically to two natural limiting cases: 1) the low frequency limit ($\omega \ll \lambda$) and 2) the high frequency limit ($\omega \gg \lambda$). The limiting forms of the spectral function are shown in Table 2. In the low frequency limit the spectrum is essentially constant with respect to frequency. The time derivative term in (4) is small, with the result that a balance exists between the damping term $[-\lambda y(t)]$ and the forcing term $[z(t)]$. The variable $y(t)$ is in phase with the forcing $z(t)$. For the high frequency case, the spectrum varies inversely as the frequency squared. The first and last terms in (4) are important, and there is a lagged relationship between the variable $y(t)$ and the forcing $z(t)$.

The two limiting cases can also be seen by taking the logarithm of (5), as is also shown in Table 2. The low frequency case is again characterized by the spectral

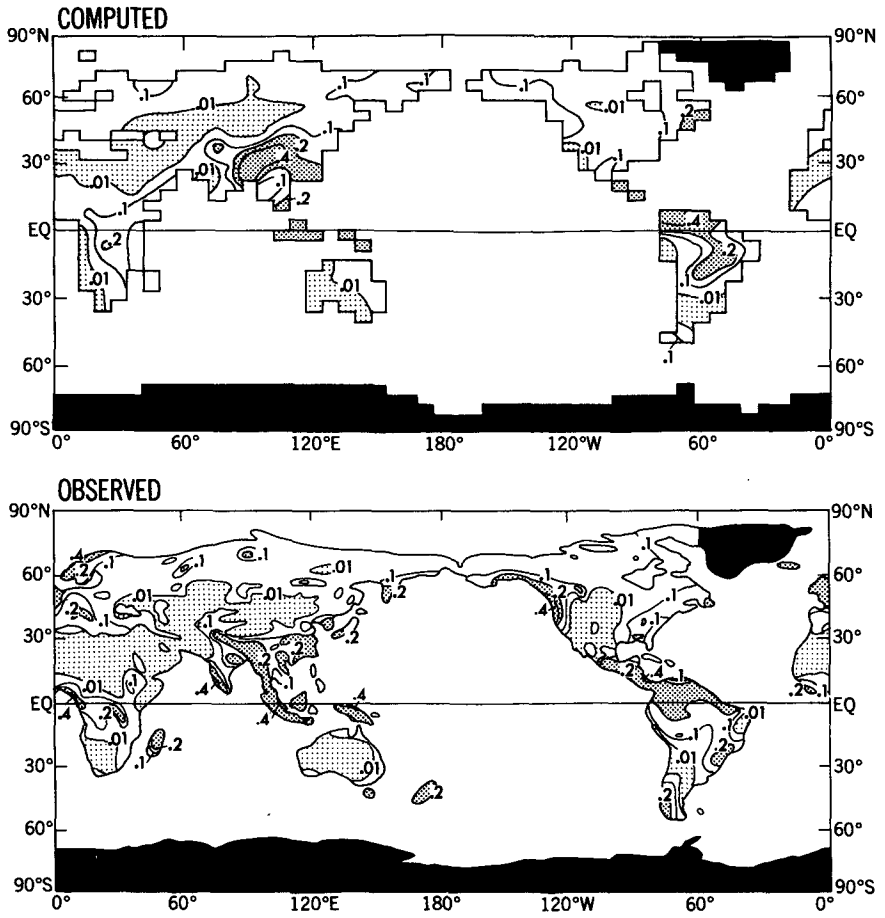

FIG. 4. Annual mean runoff rates. Units are cm d^{-1}. Lightly stippled areas represent runoff rates less than 0.01 cm d^{-1}, while densely stippled areas represent runoff rates greater than 0.2 cm d^{-1}. Solid black regions are permanently ice covered. (Top) Model computed and (bottom) estimation of the actual runoff (smoothed copy of the map constructed by Lvovitch and Ovtchinnikov 1964).

function remaining constant with respect to the logarithm of frequency. In contrast, for the high frequency case, the spectral function has a -2 slope with respect to the logarithm of frequency.

A useful quantity to characterize a red noise process is the "decay time scale." This term can be computed from the autocorrelation function of a first-order Markov process, given as (Jones 1975),

$$r(\tau) = \exp(-\lambda\tau) \tag{6}$$

where $r(\tau)$ is the autocorrelation function, τ is the lag and λ is the constant from (4).

From this equation we see that the decay time scale, defined as $1/\lambda$, is the lag at which the autocorrelation function reduces to $1/e$. The decay time scale can also be characterized from (4) as the e-folding time in the absence of forcing.

A less well-defined time scale is something we have called the "separation time scale." This time scale, intended to serve as a dividing point between the low and high frequency limits previously discussed, is defined by equating the two terms in the denominator of (5). This definition yields

$$T_s = (2\pi/\lambda) \tag{7}$$

where T_s is the separation time scale and λ is the constant from (4).

There is a physical significance to this time scale. It can be shown that for a continuous first-order Markov process, half of the total variance of the time series $y(t)$

TABLE 1. Definition of latitudinal bands used to average spectra of soil moisture, rainfall and snowmelt.

Latitude band	Range
Equatorial	4°S–9°N
Subtropical	9°–31°N
Midlatitude	31°–54°N
High latitude	54°–76°N

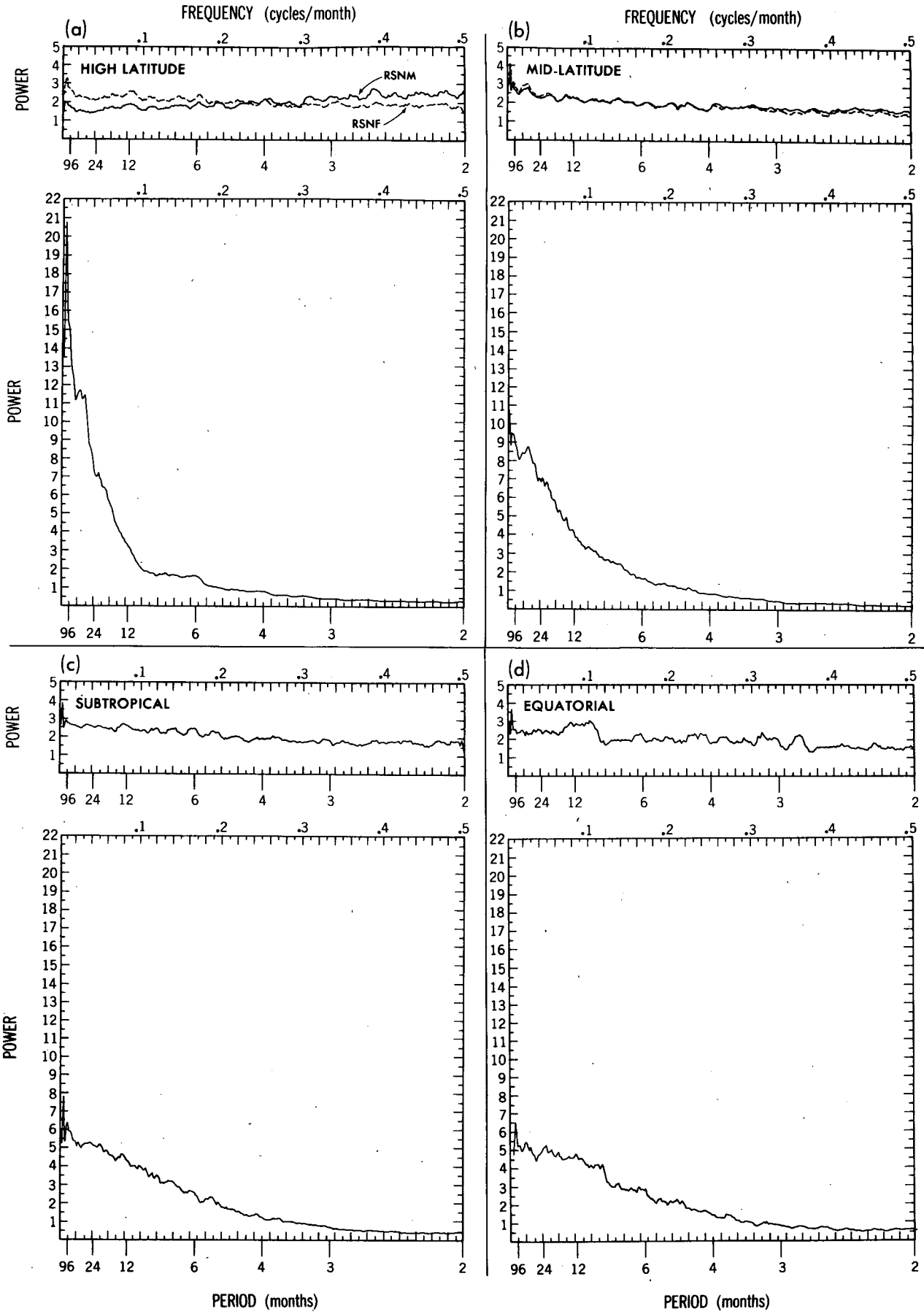
FREQUENCY (cycles/month)
(a)
HIGH LATITUDE
RSNM
RSNF
POWER
(b)
MID-LATITUDE
(c)
SUBTROPICAL
(d)
EQUATORIAL
96 24 12 6 4 3 2
PERIOD (months)

TABLE 2. Limiting forms of the analytical function $G(\omega)$ representing the spectrum of a first-order Markov process for the high and low frequency cases.

	$\omega \ll \lambda$	$\omega \gg \lambda$
$G(\omega)$	$\frac{F}{\lambda^2}$ (=const)	$\frac{F}{\omega^2}$
$\ln[G(\omega)]$	$\ln\left(\frac{F}{\lambda^2}\right)$ (=const)	$\ln(F) - 2\ln(\omega)$

is at periods longer than T_s, and half at periods shorter than T_s. This relationship only holds approximately for discrete Markov processes.

There is a mathematical resemblance between a first-order Markov process and the GFDL soil wetness parameterization, which allows model-computed soil wetness variability to be partially explained in terms of first-order Markov process theory. In order to make this resemblance more explicit, the following approximation is made: $f(w/w_{FC}) = w/w_{FC}$. It can be shown, using the zero-dimensional model discussed later, that this approximation does not substantially alter the temporal variability of soil moisture computed with this parameterization. Rewriting two equations stated earlier and using the above approximation yields

First-order Markov:

$$\frac{dy(t)}{dt} = -\lambda y(t) + z(t) \tag{4}$$

GFDL soil wetness:

$$\frac{dw(t)}{dt} = \frac{-E_p}{w_{FC}} w(t) + \text{RSNM}(t) - \text{runoff}(t). \tag{8}$$

While the correspondence between (4) and (8) is not precise, there is still substantial similarity between the forms of these two equations. The potential evaporation term in the soil wetness parameterization, divided by the field capacity, corresponds to the parameter λ in a first-order Markov process. The larger this term, the faster a moisture surplus will be dissipated and the faster the overall state returns to the mean. The RSNM time series corresponds to the white-noise forcing time series $z(t)$. The more closely the RSNM time series resembles white noise, the better the analogy of the soil moisture parameterization to a first-order Markov process. Finally, the runoff term in the GFDL soil wetness parameterization does not have an analog in a true first-order Markov process. Since the only function of the runoff term is to prevent large positive anomalies of soil wetness, this term might act to shorten the time scale for soil wetness variability in regions of frequent runoff. In the next section we will show that the geographical dependence of the temporal variability of model computed soil wetness may be approximately represented in terms of the just described controlling parameters of a first-order Markov process.

The similarity of model produced soil wetness to a first-order Markov process can be clearly seen in Fig. 6, in which the logarithm of the band averaged spectra from Fig. 5 are plotted against the logarithm of frequency. The spectra from the four bands are offset by one unit in the vertical to give a clear separation between the spectra. The thin smooth solid lines are least-squares fits of a first-order Markov process to each of the observed spectra, using the method of Reynolds (1978). One can see that the closeness of the fits strongly suggests the appropriateness of a first-order Markov process model. The high and low frequency limits for a red noise process discussed in the previous section can be clearly seen. Each spectrum is somewhat flat at low frequencies, but has a slope of approximately -2 at high frequencies.

The decay time scales of the band-averaged spectra are presented in Table 3. The longer the decay time scale, the "redder" the process, and the longer the inherent time scale of the anomalies. The increasing redness of the spectra with latitude is shown clearly. The "separation time scale" is also shown here. This time scale is roughly identified in Fig. 6 by the frequency range where the spectral function changes from being flat to sloping. This range occurs at lower frequencies for bands located more poleward. To examine how well the separation time scale partitions the spectrum into two equal variance parts, the periods which actually partition the variance into two equal parts have been computed by numerical integration of the model spectra. These values, labeled in Table 3 as the "Half variance time scales," are in good agreement with the theoretical separation time scale values.

5. Dependence of soil moisture variability on potential evaporation

The geographical dependence of soil moisture temporal variability is shown by the map of soil moisture decay time scales in Fig. 7. These values were derived by fitting a theoretical red-noise spectrum to the model soil moisture spectrum at each grid point. These decay time scales agree well with decay time scales computed using the autocorrelation function (not shown). There is a very pronounced latitudinal dependence, with soil-

FIG. 5. Composite spectra of soil moisture (solid lines in large boxes), rainfall plus snowmelt (solid lines in small boxes), and rainfall plus snowfall (dashed lines in small boxes). See text for details of compositing. (a) High latitude band, land only (see Table 1 for definition); (b) middle latitude band, land only; (c) subtropical band, land only; and (d) equatorial band, land only.

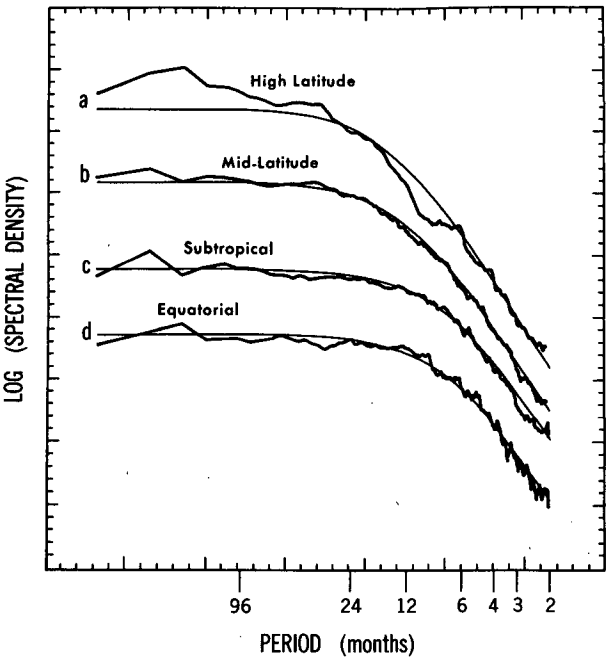

FIG. 6. Same spectra as in Fig. 2, but plotted as the logarithm of the spectrum versus the logarithm of frequency. (a) High latitude, (b) middle latitude, (c) subtropical, and (d) equatorial. The thin smooth solid lines are least squares fits of red noise spectra to the model spectra. The spectra are offset by one unit in the vertical for a clearer separation of the spectra.

moisture decay time scales increasing from typical values of two months in the tropics to over five months at high latitudes. There are also strong longitudinal variations, as evidenced by the long decay time scales over the Tibetan Plateau adjacent to the relatively short decay time scales over eastern China.

The soil moisture decay time scales, and their geographical dependence, may be viewed in terms of a first-order Markov process, as described in the previous section. According to this model, the decay time scale of a variable is equal to the inverse of the damping term. As shown in (8), potential evaporation divided by field capacity is the damping term for the GFDL soil moisture parameterization. As a result, potential evaporation and field capacity strongly influence the decay time scales of soil moisture. The geographical dependence of the temporal variability of soil moisture will therefore be examined in terms of the spatial dependence of potential evaporation. Using this relationship, an "evaporative damping time scale" (defined as the field capacity divided by potential evaporation) may be computed at each grid point. This value is an approximation of what the soil-moisture decay time scale would be if soil moisture anomalies were damped by evaporation, but not by runoff. By contrasting the field of evaporative damping time scales with the field of decay time scales derived from the time series of model soil moisture, one may evaluate to what extent evaporative damping alone is sufficient to explain soil moisture decay time scales. Where the two fields are different, some process other than evaporative damping must play an important role in determining soil-moisture decay time scales. In the ensuing discussion, the phrase "model decay time scale" refers to a decay time

TABLE 3. Soil moisture decay time scales, separation time scales, and half-variance time scales for the mean spectra from the four latitude belts defined in Table 1. Meanings of the time scales are defined in the text.

	Decay time scale (months)	Separation time scale (months)	Half-variance time scale (months)
Equatorial	1.2	7.3	7.3
Subtropical	1.2	7.7	7.7
Midlatitude	1.9	12.2	12.8
High latitude	2.5	15.6	20.0

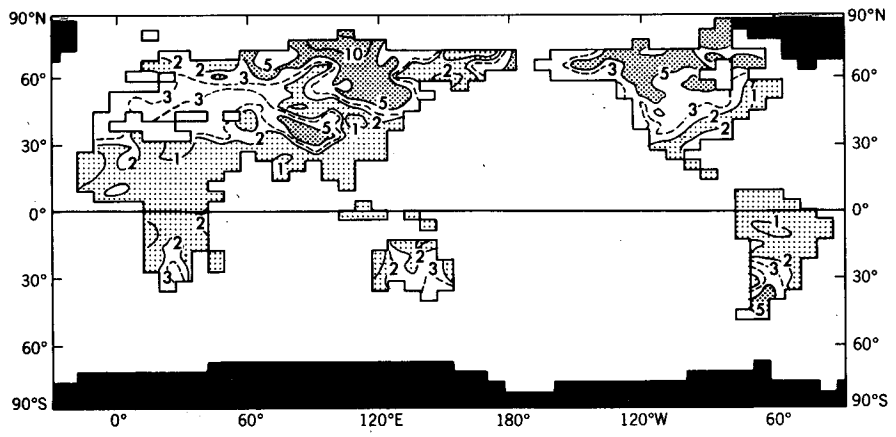

FIG. 7. Decay time scales derived from time series of model computed soil moisture. Units are months. Solid black regions are permanently ice covered.

scale computed directly from the time series of GCM soil moisture. The phrase "evaporative damping time scale" refers to a decay time scale derived from model values of potential evaporation, as outlined above.

In order to compute evaporative damping time scales, values of potential evaporation are required. Potential evaporation is an estimate of the maximum evaporation rate possible for a set of meteorological conditions. A perspective on the meaning of potential evaporation for surface hydrology can be gained by examining the surface energy balance:

$$R_{\text{net}} = \text{LH} + \text{SH} + L_i M$$

where

R_{net} net downward radiative flux at the surface
LH $[=Lf(w/w_{\text{FC}})E_p]$, latent heat flux
SH $[=\rho C_p C_D |v|(T_* - T_9)]$, sensible heat flux
$L_i M$ energy expended in melting snow cover
ρ density of air (g cm^{-3})
L latent heat of evaporation (cal g^{-1})
L_i latent heat of fusion (cal g^{-1})
M water equivalent rate of snowmelt
C_p heat capacity of the air (cal g^{-1} K^{-1})

and all other terms are as previously defined.

Rearranging and solving for E_p yields

$$E_p = (R_{\text{net}} - L_i M) \Big/ L\left[f\left(\frac{w}{w_{\text{FC}}}\right) + \frac{C_p(T_* - T_9)}{L(q_s(T_*) - q_9)}\right]. \tag{9}$$

Potential evaporation is determined by the net radiation balance at the surface, soil wetness, ground temperature, air temperature and the atmospheric mixing ratio. When a snow cover is melting, the energy expended in melting the snow is unavailable to evaporate moisture from the soil. The potential evaporation rate is decreased accordingly, as seen by the numerator in (9). Strictly speaking, the potential evaporation term in (9) is relevant to sublimation from the snow surface when a snow cover is present, and not for evaporation

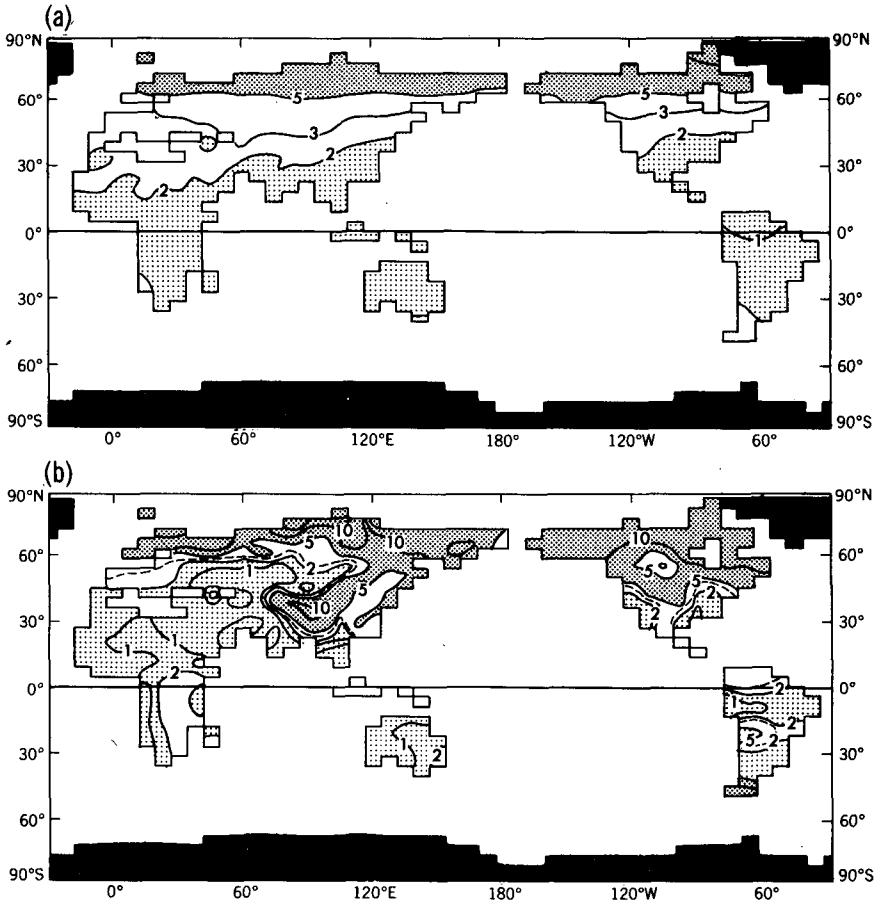

FIG. 8. Evaporative damping time scales for soil moisture, as defined in the text. Units are months. Solid black regions are permanently ice covered. Computed from potential evaporation data derived (a) using Budyko's radiation balance method and (b) using the exact form of (9).

from the soil underlying the snow. This factor is discussed later.

It is clear from (9) that potential evaporation is strongly dependent on the net radiation balance at the surface. To examine this dependence explicitly, one can compute a potential evaporation field from (9) using annual mean net radiation data, but setting $f(w) = 1$ (i.e., soil is saturated), $(T_* - T_9) = 0$ (i.e., sensible heat flux is negligible), and $M = 0$ (i.e., no energy is expended in melting snow). In such a case, (9) reduces to $E_p = R_{net}/L$. This is the definition of potential evaporation given by Budyko (1974). In Fig. 8a are shown evaporative damping time scales computed using potential evaporation values derived in this fashion. This field demonstrates the approximate dependence of the temporal variability of soil moisture on the net radiation balance at the surface. A smooth poleward increase of these time scales is observed, consistent with the smooth latitudinal gradient of the annual mean net radiation field (not shown). Large values of net radiation at lower latitudes are consistent with large potential evaporation values, and thus short evaporative damping time scales. Physically, larger values of net radiation at lower latitudes denote a greater amount of energy available for evaporation, and thus allow larger potential evaporation rates. Soil moisture anomalies at low latitudes may therefore be dissipated more rapidly and are characterized by short decay time scales. The opposite situation occurs at high latitudes, where small net radiation values permit only very low rates of evaporation, resulting in the slow dissipation of soil moisture anomalies and long decay time scales.

There are substantial differences, however, between Figs. 7 and 8a. For example, the long decay time scales seen over the Tibetan Plateau in Fig. 7 are not present in Fig. 8a. The potential evaporation values used to derive the field in Fig. 8a were only approximate values, based only on net radiation data. Quantities other than the net radiation balance at the surface also affect potential evaporation values and would thus influence these evaporative damping time scales.

Values of potential evaporation may be computed without approximation from (9). The potential evaporation values thus computed were annually averaged and used to compute the evaporative damping time scales shown in Fig. 8b. This figure bears a much stronger resemblance to the distribution of model decay time scales shown in Fig. 7. In addition to the poleward increase of evaporative damping time scales, longitudinal variations are also observed in Fig. 8b. In particular, the region of large decay time scale values over the Tibetan Plateau is captured well by this technique. These results demonstrate that on an annual-mean basis, potential evaporation is the primary control on the time scales of soil moisture variability over large regions of the globe.

The differences between the evaporative damping time scales in Figs. 8a and 8b, which are direct results of the different methods used to compute potential evaporation in each case, are indicative of meteorological factors other than the net radiation balance at the surface which affect potential evaporation. There are two distinct types of regions in which substantial differences between the two fields of evaporative damping time scales occur. In many arid regions of the globe, such as the Saharan desert and the central Asian arid zone, high ground surface temperatures and low soil moisture values produce very large potential evaporation rates, as can be inferred from (9). The technique used to compute Fig. 8a did not take these factors into account. In those areas, soil moisture anomalies are rapidly damped by evaporation, and the decay time scales for such regions are shorter in Fig. 8b than in Fig. 8a.

In mountainous and high latitude regions, such as the Tibetan Plateau and the poleward areas of North America and Asia, the decay time scales are longer in Fig. 8b than in Fig. 8a. These areas are snow covered for a substantial fraction of the year. Over these regions, a relatively large amount of the annual mean net radiation surplus at the surface is used to melt snow. As seen in (9), energy used to melt snow decreases the mean potential evaporation rate, thereby lengthening model decay time scales in regions where snow cover is frequent. In short, the decay time scales of soil moisture are longer for regions that are snow covered for a substantial fraction of the year.

A small ambiguity arises in connection with the computation of potential evaporation when the soil is covered with snow. As previously stated, the potential evaporation values computed with (9) are actually relevant to sublimation from the snow surface. However, because our interest is with evaporation from the soil, we would like to compute potential evaporation values relevant to evaporation from the soil underlying the snow. In this regard, there is a model constraint that evaporation from soil that is covered with snow is zero. Therefore, it would be more appropriate under such circumstances to set the numerator in (9) equal to zero when a snow cover exists. This would then make the potential evaporation equal to zero, consistent with the model constraint. This turns out to be unnecessary. Most of the radiation incident upon a snow covered surface is either reflected or used to melt snow. Thus, the numerator in (9) is approximately zero, making potential evaporation values negligible when a snow cover is present. The potential evaporation values actually computed from (9) are virtually identical to those computed using (9) but setting the potential evaporation to zero when a snow cover was present. Thus, the decay time scales shown in Fig. 8b are similar to those computed for the soil layer and are appropriate for comparison to Fig. 7.

There are still discrepancies between Figs. 7 and 8b that are not explicable in terms of the spatial variability of potential evaporation. These differences will be ex-

amined in a subsequent section and will be shown to result from the effects of runoff.

The above discussion of the spatial variability of evaporative damping time scales has utilized the relationship that evaporative damping time scales are defined as the field capacity divided by potential evaporation. Because the field capacity used in the GCM does not vary with location, the spatial variability of evaporative damping time scales in the model is entirely due to the spatial variability of potential evaporation. A more realistic simulation of ground hydrology might include field capacities that vary by location. The soils in arid regions would have small field capacities, while the soils of tropical rainforests would have large field capacities. The principal effect of such a change would probably be a reduction of evaporative damping time scales in arid regions, such as central Asia, where decay time scales are already short. However, the essential features of the overall pattern of soil-wetness evaporative damping time scales would probably not change substantially.

6. Variability of soil moisture computed with a zero-dimensional model

While the geographical dependence of soil moisture temporal variability on potential evaporation has been demonstrated in the previous section from GCM data, examination of (1) suggests that evaporative damping is not the only control on model soil-moisture temporal variability. The runoff process also removes moisture from the soil, and its effect on the temporal variability of soil moisture should be considered. Therefore, a zero-dimensional model of soil moisture, completely separate from the GCM, was employed to directly assess the dependence of the temporal variability of soil moisture on both runoff and potential evaporation.

The zero-dimensional model used is constructed from the following equation:

$$\frac{dw(t)}{dt} = -E_p f\left(\frac{w(t)}{w_{FC}}\right) + \text{Rainfall}(t) - \text{Runoff}(t) \quad (10)$$

where E_p is a constant value of potential evaporation (cm d^{-1}), $f[w(t)/w_{FC}]$ is as defined by (3), $w(t)$ is soil moisture (cm) and w_{FC} = 15 cm (field capacity).

This equation is a slightly modified form of the GFDL soil wetness parameterization. The modifications are that 1) the potential evaporation term (E_p) is constant, and 2) snow is not taken into consideration. These modifications were made to simplify and clarify the interpretation of the results. Inputs to the model consist of a constant value of potential evaporation, and a time series of rainfall. Numerical integration of (10) yields output time series of soil moisture and runoff.

The required model input time series of rainfall is generated using the method of Katz (1977). According to this method, a sequence of wet and dry days is generated as a two state Markov process, with fixed probabilities governing the transitions between the two states. For each day that is called "wet," the amount of rainfall ascribed to that day is drawn from a gamma distribution (Johnson and Kotz 1970). For simplicity, we use a slightly modified version of Katz's method in that precipitation values are drawn from the same gamma distribution regardless of whether the preceding day was wet or dry. The fixed parameters of this gamma distribution are usually derived from observed rainfall data. For all experiments, model parameters published by Katz (1977), derived from observed precipitation records at State College, Pennsylvania, were used in the rainfall model. Experiments have shown that small changes in the rainfall model parameters do not appreciably change the spectrum of the output rainfall time series. It was felt that the principal results from the zero-dimensional model were fairly general and did not depend on the particular rainfall time series used. While the precise time series of rainfall was not duplicated for each run, the statistics of the precipitation process used were the same for all experiments. This rainfall model, as well as the soil moisture model, is nonseasonal (i.e., the model parameters do not vary in time).

Using a time step of one day, the model is integrated for 5 years to establish a statistical equilibrium, and then for 50 years to generate a dataset for analysis. For all experiments the soil is initially completely dry. Analyses were performed on daily data.

Because the statistics of the time series of rainfall were identical for all experiments, the two independent model parameters are the mean rainfall rate and the potential evaporation rate. A number of experiments were therefore run for varying values of potential evaporation and mean precipitation rate. Increasing the mean precipitation rate while keeping potential evaporation constant increases the frequency and magnitude of runoff. Since the output soil moisture spectra were red and displayed no obvious periodicities, a decay time scale value, as discussed earlier, was deemed an adequate quantity to characterize each individual output soil moisture spectrum. For each set of experiments with a fixed precipitation rate, a decay time scale value was computed for various rates of potential evaporation.

Soil-moisture decay time scale values, denoted by the solid lines, are plotted as a function of potential evaporation in the top half of Fig. 9 for two sets of experiments with different mean precipitation rates. For values of mean potential evaporation substantially greater than the mean precipitation rate, the zero-dimensional model decay time scales are quite similar to those predicted from a first-order Markov process (not shown). For these parameter values, the GFDL soil wetness parameterization behaves much like a first-order Markov process, with the value of potential evaporation determining the decay time scale of soil

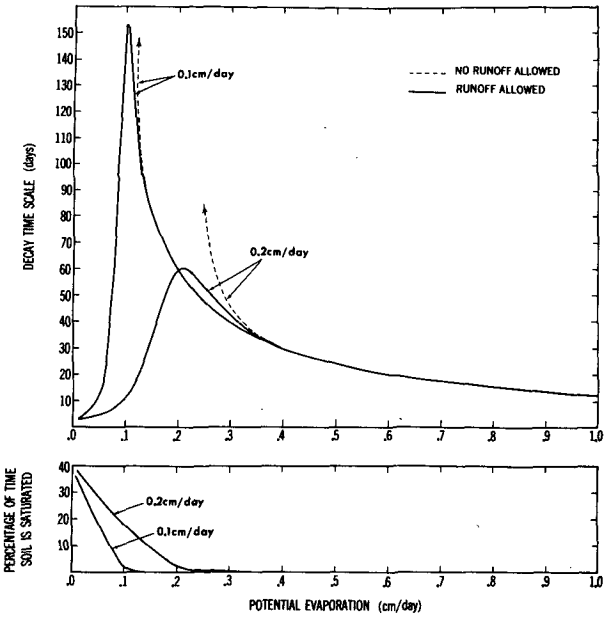

FIG. 9. (Top) Dependence of soil moisture decay time scale on potential evaporation as computed with the zero-dimensional model. The solid lines are for sets of experiments using the GFDL soil moisture parameterization, while the dashed lines are for experiments using the GFDL soil moisture parameterization modified so that runoff is not allowed to occur. The mean precipitation rates for each set of experiments are indicated. (Bottom) Percentage of days on which runoff occurs for the same experiments as in the top portion of the figure (the experiments with runoff allowed). The mean precipitation rates for each set of experiments are indicated.

moisture. The runoff term, as expressed in the lower half of the figure by the percentage of days on which runoff occurs, is virtually zero when the potential evaporation value is substantially greater than the mean precipitation rate.

For values of potential evaporation less than and approximately the same as the mean precipitation rate, a different behavior is seen. Decay time scales reach a maximum when the potential evaporation rate is close to the mean precipitation rate and drop off sharply with decreasing potential evaporation values. The percentage of days on which there is runoff increases rapidly with decreasing potential evaporation values for a fixed mean precipitation rate.

The behavior of the decay time scale curves for values of potential evaporation less than and approximately the same as the mean precipitation rate demonstrates the effect that the runoff process has on soil moisture temporal variability. By preventing excessive positive anomalies of soil moisture, the runoff process hastens the return of soil moisture values to their mean state, thereby shortening the average duration of positive soil moisture anomalies. Frequent runoff shortens soil moisture decay time scales considerably from what they would be if evaporation were the only mechanism removing moisture from the surface. Thus, frequent runoff leads to very short decay time scales, as seen for regions of the curves in Fig. 9 with potential evaporation rates less than and approximately the same as the mean precipitation rate.

The effect of the runoff process can be directly seen by examining the results of two additional sets of zero-dimensional model experiments as represented by the dashed lines. For these experiments, the model was altered so that runoff was not allowed to occur. There was no upper limit on the amount of moisture present in the soil. Thus, the differences in decay time scales, as indicated by the differences between the solid and dashed lines for the same mean precipitation rates, are entirely due to the effect of runoff. These results show that for values of the ratio of potential evaporation to precipitation which exceed approximately two, there is very little shortening of decay time scales due to runoff. However, for smaller values of this ratio, runoff can be quite effective in reducing decay time scales. For values of this ratio between one and two we see a large gap between the corresponding dashed and solid lines, with the gap becoming larger for smaller values of potential evaporation. This indicates the increasingly important role for runoff at lower values of potential evaporation. For these parameter ranges, the models with runoff have shorter decay time scales than those without runoff.

As the potential evaporation rate approaches the mean precipitation rate, however, the decay time scales corresponding to the model without runoff become extremely long (indicated by the arrows on the dashed lines). For these parameters, the soil moisture value is frequently greater than 11.25 cm, which implies from (3) and (10) that the rate of evaporative damping is constant. In effect, there is no longer a negative feedback between the soil moisture anomalies and evaporative damping, with the result that soil moisture anomalies may persist for a very long time.

For the experiments without runoff, decay time scales are not defined for values of potential evaporation less than the mean precipitation rate. For such cases, the amount of moisture in the soil grows without bound, since the mean precipitation rate exceeds the mean rate of evaporation.

Two natural regimes of soil wetness variability are thus seen to exist; they are defined by the ratio of the potential evaporation rate (E_p) to the mean precipitation rate (P_{cp}). For values of E_p/P_{cp} greater than one, there is ample energy for the removal of moisture from the surface by evaporation. The rate at which anomalies of soil moisture are damped, and thus the overall temporal variability of soil moisture, is governed by the value of potential evaporation. A different dependence is seen for values of E_p/P_{cp} less than one. Because there is insufficient energy (as measured by potential evaporation) for evaporation to balance the mean precipitation rate, a hydrologic balance necessitates frequent runoff. This process shortens soil-wetness decay time

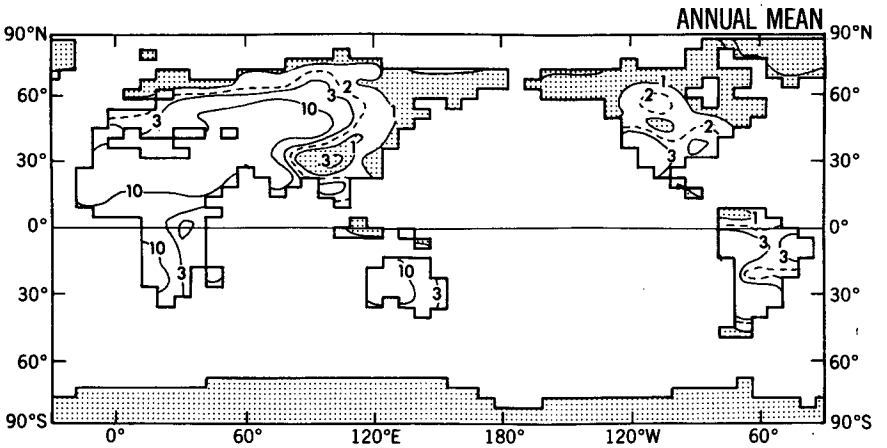

FIG. 10. Map of the ratios of annual mean potential evaporation to annual mean precipitation for model data. Areas where the ratio is less than 1.0 are stippled.

scales from those that would occur if evaporation were the only mechanism removing moisture from the surface.[1]

It should be emphasized that the values of E_p and P_{cp} are the primary determinants of the characteristics of soil moisture temporal variability. Runoff is a residual process, a result of values of E_p/P_{cp} less than one, and occurs only because of the requirement of a surface hydrologic balance.

The above results may be sensitive to the type of soil wetness parameterization employed. Therefore, additional zero-dimensional model experiments were conducted employing a distinctly different soil wetness parameterization. These results are discussed in appendix B.

7. Dependence of soil moisture temporal variability on runoff

The effect of the runoff process on soil moisture decay time scales may also be seen from GCM data. The ratios of annual mean potential evaporation to precipitation are shown in Fig. 10. Regions where this ratio is less than one are regions of frequent runoff, as can be verified by comparing Figs. 4 and 10. The discussion in the previous section suggests that these areas should also have soil moisture decay time scales which are shortened due to runoff effects. A comparison of Figs. 7 and 10 reveals that most regions possessing soil moisture decay time scales shorter than their respective zonal means are also characterized by values of E_p/P_{cp} less than one, and are thus characterized by frequent runoff. The far northeast of Siberia is a good example of this effect, as well as the coast of Alaska and the area immediately to the east of the Tibetan Plateau.

The effect of runoff on soil moisture decay time scales may be more directly seen by comparing Figs. 7 and 8b. As previously discussed, Fig. 8b is a map of evaporative damping time scales computed with the assumption that evaporation is the only mechanism removing moisture from the soil. The model-computed soil moisture decay time scales in Fig. 7, however, take both evaporative damping and runoff into account. Therefore, some of the differences between the two fields are indicative of the shortening of soil moisture decay time scales due to runoff. Typically, the regions in Fig. 7 with soil moisture decay time scales considerably shorter than those in Fig. 8b are also characterized in Fig. 10 by E_p/P_{cp} values less than one, suggesting that the runoff mechanism is responsible for the differences.

8. Seasonal aspects of soil moisture temporal variability

While most of the foregoing discussion was based on annual mean data, there are substantial seasonal changes in potential evaporation and in the ratio of potential evaporation to precipitation. These changes imply that for any given region, not only may the time scale of soil moisture variability change with season, but the mechanism governing that decay time scale may also change.

Potential evaporation fields averaged over the months of December–February, as well as over June–August are shown in Fig. 11. At middle and high latitudes a very large seasonal cycle of potential evaporation corresponds to the large seasonal cycle of net radiation at the surface. These changes imply that soil-moisture decay time scales are short in summer and

[1] The dimensionless quantity E_p/P_{cp} was used by Eagleson (1978) to describe variations in the surface latent heat flux. We have used this quantity to characterize the temporal variability of soil moisture computed in a GCM.

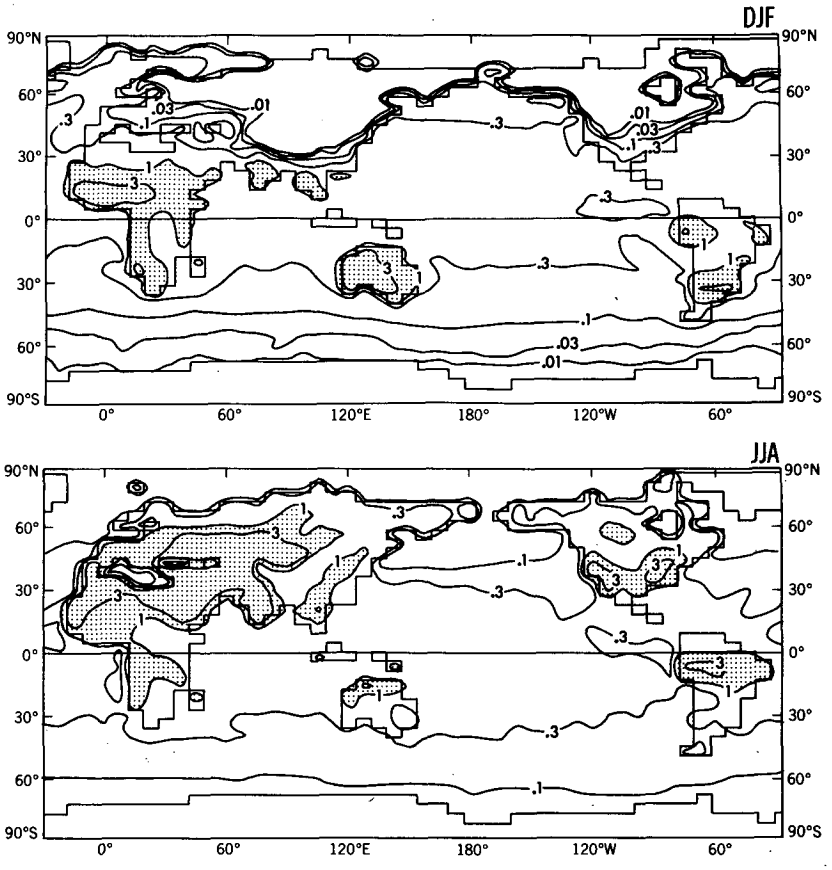

FIG. 11. Model potential evaporation computed from (9), as described in the text. Units are cm d^{-1}. Stippled areas possess values greater than 1 cm d^{-1}. (Top) December–February average (DJF) and (bottom) June–August average (JJA).

long in winter. Physically, soil moisture anomalies are rapidly dissipated in summer when there is an abundance of radiational energy available for evaporation at the surface. In winter, the small amount of radiational energy available for evaporation at the surface dictates that soil moisture anomalies are dissipated very slowly.

Figure 12 shows the mean ratio of potential evaporation to precipitation averaged over the months of December–February, as well as over the months of June–August. In winter the values of E_p/P_{cp} are less than one over large areas, suggesting that the runoff process strongly affects soil moisture decay time scales. In summer, however, the values of E_p/P_{cp} are greater than one over most areas, suggesting that potential evaporation is the dominant control on soil-moisture decay time scales. It should be noted (not shown) that for winter, soil-moisture decay time scales can still be very long despite the influence of the runoff process. Evaporative damping time scales are exceedingly long in winter due to the very small net radiation values. Reduction of these time scales by runoff still leaves soil-moisture decay time scales that are quite long.

9. Surface air temperature variability

A fundamental question of interest in studying model soil moisture variability is how that variability affects the atmosphere. That question has been addressed by performing a second long-term GCM integration, employing the same model but with altered boundary conditions. This second experiment will be called the "noninteractive" case, as opposed to the first experiment, the "interactive" case. In the noninteractive experiment, daily soil wetness, snow cover and land albedo values are prescribed at each grid point based on the climatological values computed from the first model run. These values are based on 5-day means, and interpolated to daily values. Thus, much of the hydrologic interaction between the atmosphere and land surface has been removed. By comparing the differences in atmospheric variability between the two experiments, one can assess the relative contributions of interactive hydrologic processes to atmospheric variability.

Based on heat balance considerations we might expect soil moisture anomalies to have a substantial effect

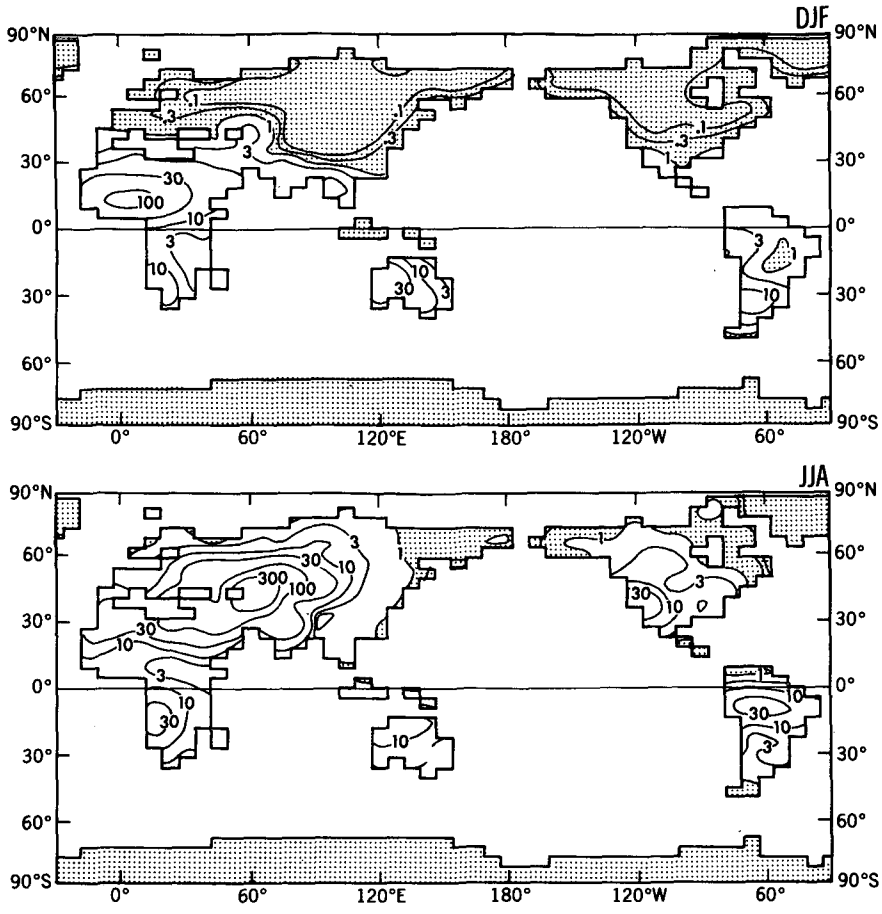

FIG. 12. Map of the ratios of potential evaporation to precipitation for model data. Stippled areas denote a ratio greater than 1.0. (Top) December–February average (DJF) and (bottom) June–August average (JJA).

on surface air temperatures. Thus, the variances of monthly mean Northern Hemisphere summer (JJA) surface air temperature have been computed for the two experiments. These variance maps, along with the ratio of the variance of the interactive experiment to the variance of the non-interactive experiment, are shown in Fig. 13. The zonal means of the variances are shown in Fig. 14. Table 4 lists the variances for the two experiments, as well as the percentage by which the variance of surface air temperature in the interactive case increased over the variance of surface air temperature in the noninteractive case.

It is clear, both from the maps and the table, that the variance of the interactive case is much larger than the noninteractive case, indicating the substantial role interactive soil moisture plays in summer surface air temperature variability. The magnitude of this increase is latitudinally dependent. The zonal means show that the increase of variance for the interactive case is largest at low and middle latitudes of the Northern (summer) Hemisphere, and very small at high latitudes. As a fraction of the variance of the noninteractive case, the changes in variance are largest at low latitudes.

The specific regional differences are quite interesting. At low and middle latitudes there are large changes between the two experiments. A maximum of variance appears over the eastern portion of the United States in the interactive run that was not present in the noninteractive run. Similarly, over northern Africa, southern Europe, south Asia and Australia, there are substantial increases in variance in the interactive run. Changes in the Southern Hemisphere are generally small.

There is a seasonal dependence of the increase in surface air temperature variance between the two experiments. Figure 15 is similar to Fig. 13, but computed for the Northern Hemisphere winter season (DJF). While the overall magnitude of the variance of surface air temperature is larger for the winter months in both experiments, the relative increase in variance of the interactive experiment over the noninteractive experiment is much smaller in winter than in summer. De-

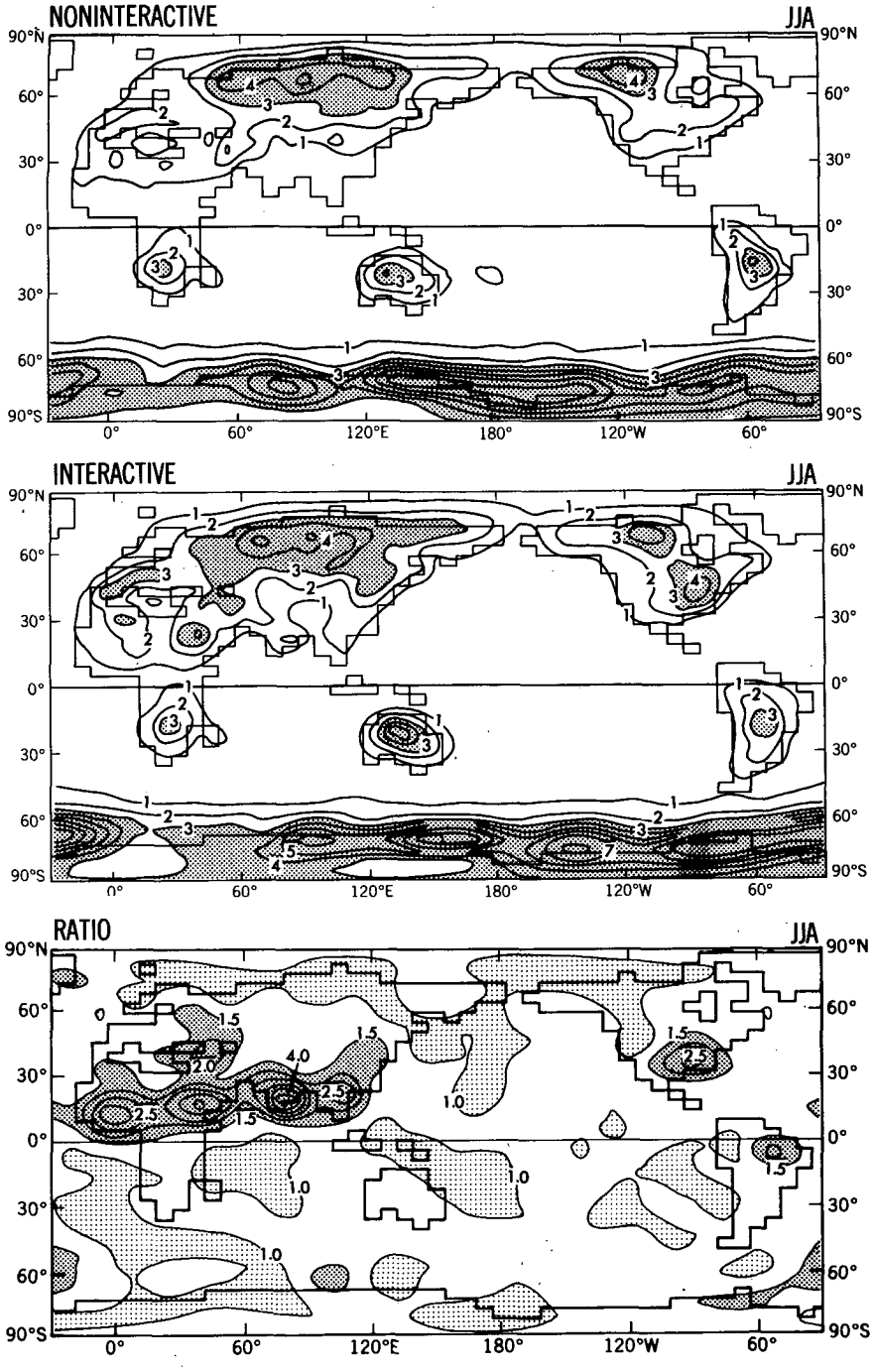

FIG. 13. (Top) Variances of monthly mean surface air temperature as computed by the noninteractive experiment for June–August. Units are (°C^2). (Middle) Same as top panel but for the interactive experiment. (Bottom) Ratio of the variance of surface air temperature for the interactive experiment to the noninteractive experiment for June–August. Areas where the ratio exceeds 1.5 (i.e., where the increase of variance between the two experiments exceeds 50%) are densely stippled. Areas where the ratio is less than 1.0 are lightly stippled.

spite shifts in the spatial patterns of the variance between the two experiments, the areal mean Northern Hemisphere surface air temperature variance over land is very similar for the two experiments. Interactive soil moisture does not appear to make a substantial contribution to winter surface air temperature variability.

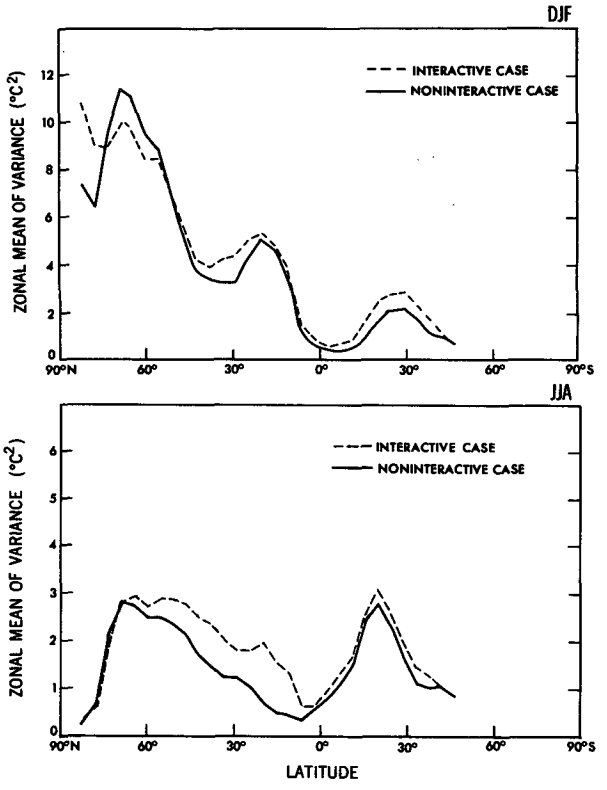

FIG. 14. Zonal means of surface air temperature variance. (Top) December–February (DJF) and (bottom) June–August (JJA).

These results may be interpreted in terms of the surface energy balance. As a result of the model constraint that no heat be stored in the ground, all energy supplied to the surface must be balanced by energy removed from the surface. The net radiational input to the surface must therefore be balanced by the outgoing fluxes of latent and sensible heat. While the sum of the latent and sensible heat fluxes is determined by the need to balance the radiational input, the partitioning of the total outgoing heat flux into latent and sensible heat fluxes is strongly influenced by the value of soil wetness. In general, for a given net radiation, the larger the value of soil wetness, the larger the value of the latent heat flux and the smaller the value of the sensible heat flux. Through this partitioning of the total outgoing heat flux and because surface air temperature is strongly related to the surface flux of sensible heat, interactive soil wetness enhances atmospheric variability. Fluctuations in soil wetness produce changes in the latent and sensible heat fluxes, thereby enhancing the variance of surface air temperature.

In this context, it is not surprising that the noninteractive experiment has generally smaller surface air temperature variability than the interactive experiment. Because soil wetness is prescribed in the noninteractive run, the partitioning of the outgoing energy flux into latent and sensible heat fluxes, as measured by the ratio of the sensible heat flux to the latent heat flux at the surface (Bowen's ratio), does not vary much in time. This constraint on the Bowen ratio reduces the temporal variations of the sensible heat flux, thereby reducing the variance of surface air temperature in the noninteractive experiment relative to the interactive experiment. In contrast, soil wetness values in the interactive run are free to vary. The Bowen ratio can vary substantially, thereby allowing latent and sensible heat fluxes to have large fluctuations. The variance of these fluxes enhances the variance of surface air temperature in the interactive experiment relative to the noninteractive experiment.

It is important to note that the flux of latent heat is directly proportional to the potential evaporation value under conditions of sufficient moisture. Therefore, the magnitude of the influence of soil moisture anomalies on low level atmospheric temperature is also proportional to the value of potential evaporation. This relationship can be used to explain both the latitudinal and seasonal dependence of changes in surface air temperature variance between the two experiments.

The winter and summer mean maps of potential evaporation computed using the direct method were shown in Fig. 11. It is clear that for the Northern Hemisphere summer months there is a strong dependence of potential evaporation on latitude. It has also been shown that the change in surface air temperature variance between the two experiments has a latitudinal dependence. These two features are strongly related. It can be seen from a comparison of Figs. 11, 13 and 15

TABLE 4. Variances of surface air temperature for the months of June–August for the noninteractive experiment (top) and for the interactive experiment (middle). Units are (°C²). The percentage increase of the variance of surface air temperature of the interactive experiment over the noninteractive experiment is shown in the bottom portion.

	Land	Sea	Total
	Variances of surface air temperature for the noninteractive experiment		
NH mean	1.602	0.398	0.874
SH mean	2.414	0.980	1.257
Global mean	1.868	0.731	1.066
	Variances of surface air temperature for the interactive experiment		
NH mean	2.175	0.430	1.120
SH mean	2.672	1.092	1.397
Global mean	2.338	0.809	1.259
	Percentage increase of the variance of surface air temperature of the interactive experiment over the noninteractive experiment		
NH mean	36	8	28
SH mean	11	11	11
Global mean	25	11	18

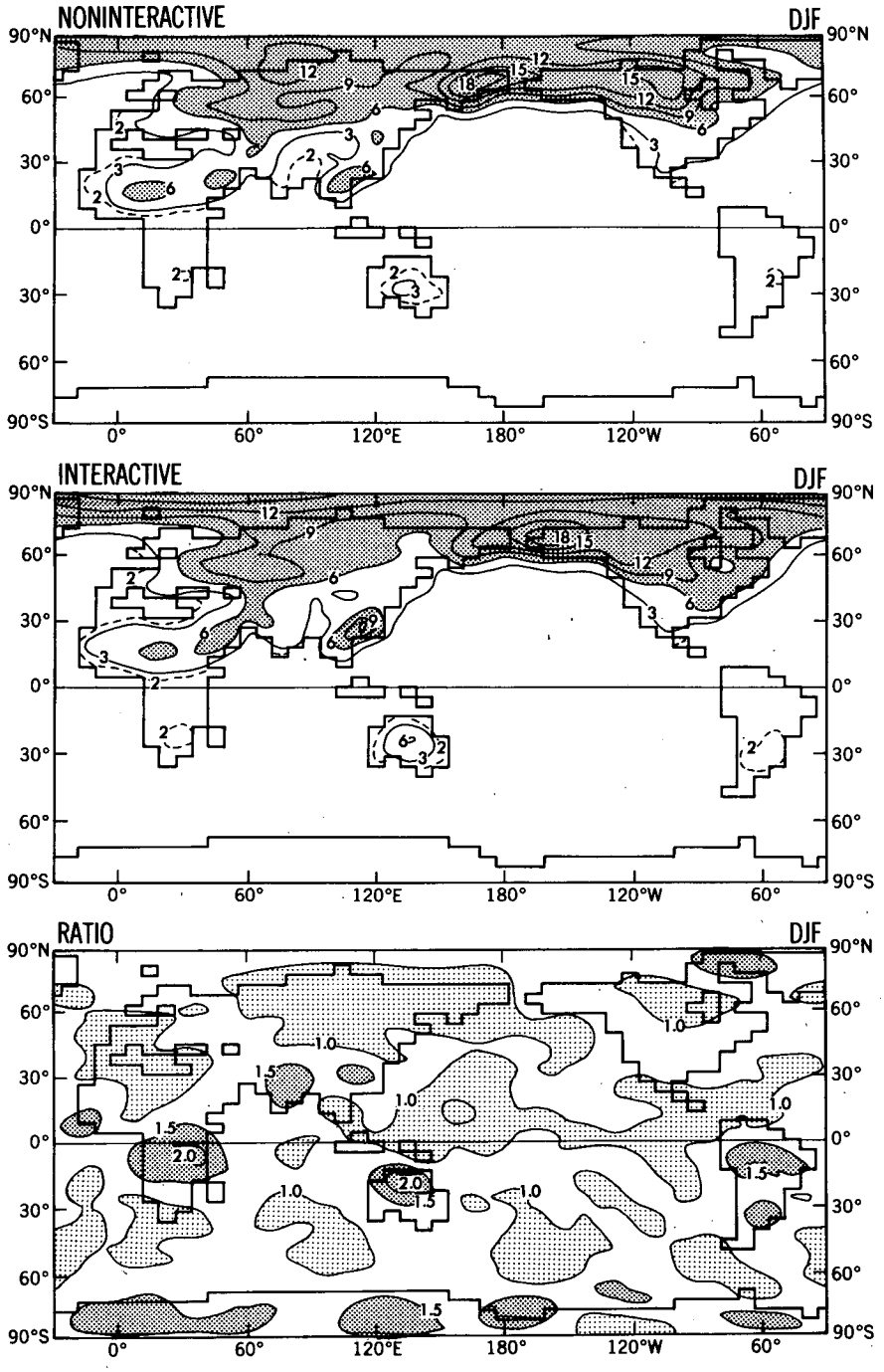

FIG. 15. As in Fig. 13, but for December–February.

that the increase of surface air temperature variance in the interactive run relative to the noninteractive run is larger for regions and seasons with large potential evaporation values. This is a result of the fact that the flux of latent heat is proportional to the potential evaporation value. For a fixed change in soil wetness, regions with large potential evaporation values will experience larger changes in their latent and sensible heat fluxes than regions with small potential evaporation values. Large changes in these fluxes result in large values of surface air temperature variance, as previously discussed. Thus, the increase of surface air temperature variance for the interactive experiment relative to the noninteractive experiment tends to be large for loca-

tions and seasons with large potential evaporation values. Principally, these occur in the tropics and the summer hemisphere extratropics. The very small changes in surface air temperature variance at high latitudes in summer and at middle and high latitudes in winter partly result from the small potential evaporation values found there.

Although these differences in variability are for only one model field, these analyses nevertheless demonstrate the potential importance of land surface processes to low frequency atmospheric variability.

10. Discussion and conclusions

It has been shown that time series of soil moisture computed in a general circulation model (GCM) contain substantial amounts of variance at low frequencies, with more than half of the total variance residing at periods of one year or longer for many middle and high latitude locations. Soil moisture has variability on both the intraseasonal and interannual time scales. Time series of soil moisture anomalies have spectra which are similar to spectra derived from red-noise processes. The redness of these spectra, and thus the overall time scale of soil moisture variability, generally increases with latitude. An exception, however, is that in regions where the ratio of annual mean potential evaporation (E_p) to annual mean precipitation (P_{cp}) is less than one, which are also regions characterized by frequent runoff, soil moisture anomalies tend to have fairly short time scales. The redness of the soil moisture spectra is in contrast to the white noise character of the time series of rainfall plus snowmelt.

Physically, the soil layer acts as an integrator of the rainfall plus snowmelt time series, transforming the input white noise forcing into an output soil moisture time series which is similar to red noise. For short time scales there is a lagged relationship between soil moisture and precipitation. Anomalies of soil moisture are strongly influenced by past precipitation anomalies. However, the dissipative processes of evaporation and runoff do not allow anomalies of soil moisture to persist indefinitely. At longer time scales, current soil moisture is hardly affected by past precipitation and is determined such that the balance between precipitation and evaporation is maintained.

It has also been shown that the temporal variability of soil moisture is influenced by two different mechanisms. The ratio of E_p to P_{cp} determines which mechanism is dominant. When this ratio is greater than one, the rate of evaporative damping, proportional to the potential evaporation value, strongly influences the temporal variability of soil moisture. Large potential evaporation values at low latitudes, a result of the large net radiative flux at the surface, allow soil moisture anomalies to be rapidly damped. The time scales of soil moisture variability are thus quite short. At higher latitudes, however, small potential evaporation values, a result of the small net radiative flux at the surface, permit only a very slow dissipation of soil moisture anomalies. Time scales of soil moisture variability are thus quite long. A longitudinal dependence of soil moisture time scales is also observed. Variations in potential evaporation, resulting from differing mean values of soil wetness and temperature, account for some of this dependence.

A different type of variability is observed when the ratio of E_p to P_{cp} is less than one. Under these conditions, the maintenance of a hydrologic balance at the ground surface results in frequent saturation and runoff. A consequence of this is that decay time scales of soil moisture are shortened from what they would be if evaporation were the only mechanism removing moisture from the surface. In such regions, decay time scales can be quite short, even where potential evaporation values are very small.

In general, the temporal variability of GCM computed soil moisture is strongly influenced by potential evaporation and precipitation. For seasons and locations where the ratio of E_p to P_{cp} is greater than one, potential evaporation determines the decay time scales of soil moisture. For seasons and locations where this ratio is less than one, frequent runoff, dictated by the hydrologic balance, is the mechanism by which the decay time scales of soil moisture are substantially shortened. To a first approximation, the persistence of soil moisture anomalies over the majority of Northern Hemisphere land areas is governed by potential evaporation during summer.

There is a striking analogy between the role ascribed here to soil wetness and the role others have ascribed to sea surface temperature anomalies. As mentioned earlier, it has been shown that sea surface temperature anomalies are well modeled as a first-order Markov process over large regions of the oceans (Reynolds 1978). The ocean acts as an integrator of high frequency atmospheric thermal forcing. This integration process gives the ocean a long memory, which then can reinject a low frequency signal into the atmosphere. The soil layer may play a similar role by integrating white-noise precipitation forcing and creating a red-noise time series of soil moisture anomalies. However, the time scales of the soil moisture anomalies are shorter than the time scales of sea surface temperature anomalies.

The explicit dependence of the temporal variability of soil wetness anomalies on potential evaporation is based on the analogy between the GFDL soil moisture parameterization and a first-order Markov process. According to this analogy, the spectrum of precipitation anomalies should be similar to white noise. If the precipitation spectrum is substantially different from white, then the nonwhite characteristics of the precipitation spectrum may also influence the time scales of soil wetness variability. Various feedback processes, including air–sea interaction and the influence of increasing atmospheric carbon dioxide, can enhance the

low frequency portion of the precipitation spectrum. At low frequencies, soil moisture values are determined such that an equilibrium between precipitation and evaporation is maintained, as previously discussed. Thus, the enhanced variability of precipitation at low frequencies results in the lengthening of the time scales of soil wetness variability. Such a process may have contributed to the very persistent anomalies of precipitation and soil moisture observed over the Sahel region of Africa since the 1950s. Folland et al. (1986) suggest that the influence of slowly varying sea surface temperature anomalies in the Atlantic has created very long term fluctuations of precipitation, and hence soil moisture, over portions of Africa.

While the model employed in this study does not incorporate air–sea interaction or changing concentrations of carbon dioxide, the GCM does include interactions between the land surface and atmosphere. Model analyses (not shown) have demonstrated that these interactions enhance the low frequency variability of precipitation over regions with large potential evaporation values. These results will be described in a subsequent publication.

The precipitation spectrum can also take on nonwhite characteristics in arid regions, where months can pass between rainfall events. In such cases, there may be a reduced variability of precipitation on the monthly time scale. The temporal variability of soil wetness on the monthly time scale is then largely determined by the interval between rainfall events, rather than by potential evaporation or field capacity. While analyses (not shown) have demonstrated that this situation does not occur in the model, it may be of relevance to the real climate system.

The potential impact on climate of the low frequency nature of soil moisture variability, especially in the tropics and in the middle latitudes during summer months, is substantial. Variability of soil moisture affects the atmosphere primarily through the surface heat balance. A comparison of two GCM integrations, one with interactive soil moisture and one with noninteractive soil moisture, has shown that interactive soil moisture substantially increases the variance of surface air temperature for regions with large potential evaporation values. This occurs primarily at low latitudes all year and at middle latitudes during summer months.

It should be noted, however, that the spatial scales of soil moisture anomalies will strongly influence their potential effects on the atmosphere. If anomalies are coherent only over very small spatial scales, then the soil moisture anomalies to exert a substantial, large scale influence on the atmosphere is diminished. An analysis of the model results is currently in progress to determine whether any large scale patterns of soil moisture spatial variability exist that are capable of exerting a substantial influence on the atmosphere and its variability.

Due to the simple soil moisture parameterization employed, the quantitative aspects of the results presented, particularly the decay time scales of soil moisture, should not be taken too literally. The effects of vegetation, varying soil characteristics and subsurface water flow, among others, influence the temporal variability of soil moisture in the real climate system. Nevertheless, we feel that because the GFDL soil moisture parameterization models the fundamental hydrologic processes of precipitation, evaporation, runoff and snowmelt, the mechanisms of the temporal variability of soil moisture discussed here are relevant to real hydrologic variability.

In this connection, it is important to note the intercomparison study described in appendix B. That study compares the performance of the GFDL soil moisture parameterization to that of the Goddard Institute for Space Studies (GISS) model by constructing two versions of a simple zero-dimensional model. The latter parameterization attempts to incorporate some of the physical processes neglected in the former. In spite of this, the temporal variabilities of soil moisture computed with the two parameterizations were similar in general character. Moreover, the temporal variability of soil moisture was dependent on similar physical mechanisms for both parameterizations. Thus, the mechanisms discussed here for controlling the temporal variability of soil moisture are not limited to one particular parameterization, but are of wider relevance.

There do exist, however, quantitative differences in the temporal variabilities of soil moisture computed with the two parameterizations. Such differences highlight the critical need for an improved ability to determine the accuracy of model surface hydrology parameterizations with respect to the real climate system.

Acknowledgments. The authors are grateful to A. J. Broccoli and R. J. Stouffer for guidance in the integration of the GCM. Drs N-C. Lau, Y. Hayashi, P. C. D. Milly and Prof. P. Eagleson read the first draft of the paper and made many valuable suggestions for improvement. The comments of two anonymous reviewers were greatly appreciated. The final figures were prepared by P. Tunison and his staff.

APPENDIX A

Computation of the Moisture Field

The spectral representation of any model field is truncated after summing over the basis functions corresponding to the lowest wavenumbers, the number of components retained dependent upon the resolution of the model. For a low resolution model, these basis functions are capable of representing only the largest scale features. Thus, spectrally truncated models in general, and low resolution models in particular, encounter problems in attempting to represent fields containing small spatial scale variability. These problems are a direct result of spectral truncation. While all model fields suffer from this problem, atmospheric

moisture fields are strongly affected because of their inherently small spatial scales.

Two distinct types of problems arise. First, errors due to spectral truncation may result in mixing ratio values that are less than zero. This occurs most frequently in the model at high latitudes because of the small climatological mixing ratio values found there. Since negative mixing ratio values are not physically realizable, the model's moisture field is arbitrarily adjusted to reduce the number of such occurrences.

The second type of problem occurs when errors due to spectral truncation result in mixing ratio values larger than the appropriate saturation mixing ratio values. Because of the model constraint that precipitation occurs whenever the mixing ratio exceeds the saturation mixing ratio, this error creates precipitation that is solely an artifact of the spectral truncation. This "fictitious" precipitation has no basis in the model's physics and distorts both the hydrologic cycle and diabatic heating field.

An alternate method was therefore used to compute moisture fields. While other model variables were computed using semispectral techniques, a finite difference scheme was adopted for the moisture field. This scheme consists of a prognostic equation for water vapor and a second mass continuity equation, in finite difference form, which is distinct from the original mass continuity equation in semispectral form. The "box" method of Kurihara and Holloway (1967) is employed for the finite difference computations [see their continuity equation (3.5A) and (3.6A) for the diagnostic computation of vertical velocities].

The second mass continuity equation, cast in finite difference form, is required because the divergence computed from the semispectral mass continuity equation is different from the divergence computed from the finite difference mass continuity equation. The vertical velocity fields, derived from the two different mass continuity equations, are therefore different. For consistency, the finite difference prognostic equation for water vapor uses the vertical velocities consistent with the finite difference mass continuity equation.

Model analyses have shown that the number of points with negative mixing ratios in polar regions is substantially reduced by utilizing this finite differencing technique for the moisture field. In addition, spatially smoother model precipitation fields are observed. It was felt that these changes improved the model's hydrologic simulation.

APPENDIX B

A Comparison of the Temporal Variability Inherent in the GFDL and GISS Soil Wetness Parameterizations

In order to assess the sensitivity of the temporal variability of computed soil wetness to the particular soil wetness parameterization employed, the zero-dimensional model described in the main text was modified to incorporate the Goddard Institute for Space Studies (GISS) soil wetness parameterization (Hansen et al. 1983). The GISS parameterization was chosen because it represents a significantly different class of soil wetness parameterizations possessing more than one layer. A comparison of soil wetness temporal variability results obtained using the GFDL scheme with those obtained using the GISS scheme offers some insight into the sensitivity of the output soil wetness variability to the particular soil wetness parameterization. The results are of relevance not only for this zero-dimensional model, but for general circulation models as well.

There are two main differences between the GISS and GFDL schemes; 1) the GISS scheme has two layers in the vertical which exchange moisture by a diffusion-like process, in contrast to the single GFDL layer, and 2) runoff occurs whenever there is precipitation in the GISS scheme, whereas runoff occurs in the GFDL scheme only when the entire layer is saturated. The upper layer in the GISS scheme interacts with both the atmosphere and lower layer, while the lower layer interacts only with the upper layer. Evaporation is computed in the GISS scheme as a linear function of soil wetness of the upper layer, varying from zero evaporation when the upper layer is completely dessicated to evaporation at the potential rate when the top layer is saturated. For the purpose of this comparison, all soil moisture is assumed to be in the liquid state.

The soil moisture parameterization as actually implemented in the GISS model incorporates seasonally varying vegetative effects, as well as freezing of moisture in the soil. While these processes will affect the temporal variability of soil moisture in the GISS model, they were omitted from our comparison for the sake of simplicity. We do not believe that this omission significantly affects our conclusions.

Because we wish to ascertain changes in the temporal variability of soil wetness that are a result of the additional layer in the GISS parameterization, the differences between the GFDL and GISS runoff formulations may influence such a comparison. Therefore, two versions of the GISS parameterization were employed. The first, denoted as GISS-I, incorporates runoff as actually implemented in the GISS model (model 2 as reported in Hansen et al. 1983). In this version, runoff occurs whenever there is precipitation. The second, denoted as GISS-II, is a version in which runoff occurs only when the top layer is saturated. It is hoped that a comparison of the GFDL scheme with the GISS-II scheme will be indicative of general variability differences between one and two layer soil wetness parameterizations, since the GFDL and GISS-II schemes use similar runoff formulations. It should be stated that, unless otherwise noted, both versions of the GISS scheme used the following parameters (from Hansen et al. 1983):

Upper layer water holding capacity = 2.4 cm
Lower layer water holding capacity = 12.0 cm
Diffusion time constant from upper layer to lower layer = 1 day
Diffusion time constant from lower layer to upper layer = 0 days
(The diffusion time constant of 0 days means that the model assumes that there is an active root system which instantaneously transports water from the lower layer to the upper layer when the upper layer is drier than the lower layer.)

The dependence of soil moisture decay time scales on potential evaporation and runoff was examined for the three different schemes (GFDL, GISS-I and GISS-II). For both GISS schemes, decay time scales were computed from the time series of total soil moisture, defined as the sum of the soil moisture contents of the upper and lower layers. The results are shown in Figs. B1 and B2. Figure B1 shows the decay time scales for a set of experiments with a mean precipitation rate of 0.1 cm d^{-1}, while Fig. B2 is for a set of experiments with a mean precipitation rate of 0.2 cm d^{-1}. It is clear that the overall dependence of decay time scales on potential evaporation for the two GISS schemes bears some qualitative similarity to the GFDL scheme, but with quantitative differences. As discussed in the text and as can be seen from Figs. B1 and B2, the value of the ratio of potential evaporation (E_p) to precipitation

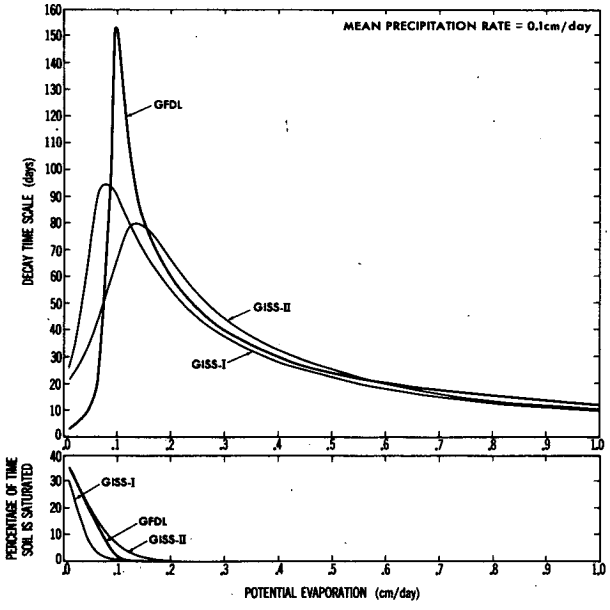

FIG. B1. (Top) Decay time scales versus potential evaporation for a mean precipitation rate of 0.1 cm d^{-1}. The heavy, solid line represents the zero-dimensional results using the GFDL soil wetness parameterization. The two lighter lines represent zero-dimensional model results using the GISS-I and GISS-II soil wetness parameterizations. (Bottom) Percentage of days on which the soil is saturated as a function of potential evaporation. For the results using the GISS parameterizations, the soil is saturated when the top layer is saturated.

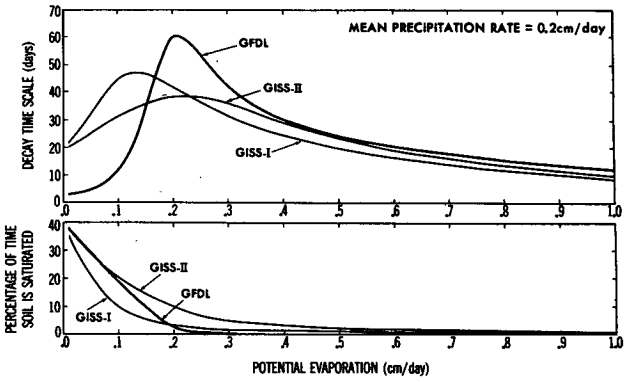

FIG. B2. Same as top of figure B2, but for a mean precipitation rate of 0.2 cm d^{-1}.

(P_{cp}) is important in describing the behaviour of the decay time scale curves. For values of E_p/P_{cp} greater than one, the decay time scale curves for both GISS schemes resemble the GFDL decay time scale curve. All three schemes show a decrease of soil moisture decay time scale with increasing potential evaporation, in a fashion similar to the theoretical Markov process described in the main text.

For values of E_p/P_{cp} substantially less than one, both GISS schemes yield longer decay time scales than the GFDL scheme. This difference is probably due to the presence of a second layer in the GISS schemes. When the GFDL single layer is frequently saturated, the dependence of daily soil moisture on the preceeding day's soil moisture is reduced. In this case, because soil moisture depends strongly on daily precipitation, which has very low autocorrelation values, the decay time scales of soil moisture are shortened. However, even when the upper layer of either GISS scheme is saturated, the lower layer is not necessarily saturated. Autocorrelation and decay time scales are thus not reduced as much as for the GFDL case. In effect, the lower layer still possesses a "memory," whereas the "memory" of the GFDL single layer scheme is erased at saturation. In this sense, the presence of a second, deeper layer in the GISS schemes, not subject to runoff, "buffers" the total system from the efforts of runoff to shorten the overall time scale of the system. It should be stated that a number of high latitude locations in the GCM with the GFDL soil wetness parameterization have decay time scales that are substantially shortened by runoff. From the above analyses, we might expect that if the GISS soil wetness parameterization were to be used, this shortening of decay time scales in regions where the value of E_p/P_{cp} is small might not be as pronounced.

The GISS-I scheme (the version employed in model 2 of Hansen et al. 1983) is seen in Fig. B1 to have decay time scales which are longer than those for GISS-II when E_p/P_{cp} is less than one. The GISS-I scheme, in addition to defining runoff to occur when the top layer

is saturated, also states that runoff occurs whenever there is precipitation. The proportion of precipitation which immediately becomes runoff is one half the fractional saturation of the upper layer. This additional runoff term effectively decreases the mean precipitation rate. It is important to note that although the total amount of runoff is larger in the GISS-I model than in the GISS-II model, the percentage of days on which the upper layer is saturated is smaller in the GISS-I model. Much of the precipitation is removed before it penetrates the soil layer. Thus, because the GISS-II model is more easily saturated than the GISS-I model for the same values of potential evaporation and precipitation, the runoff process shortens the decay time scales in the GISS-II model relative to the GISS-I model for values of E_p/P_{cp} less than one.

As discussed in section 9, interactive soil moisture may make a substantial contribution to the temporal variability of surface air temperature. The type of contribution may depend on the particular soil moisture parameterization used. In general, the upper layer of the GISS scheme, which is the layer that interacts directly with the atmosphere, is characterized by short decay time scales and large amplitude fluctuations of soil wetness. Therefore, one might speculate that interactive soil moisture computed with the GISS scheme would contribute to the variability of surface air temperature at higher frequencies, and with a larger amplitude, than soil moisture computed with the GFDL scheme.

In summary, the GISS and GFDL soil wetness parameterizations possess qualitative similarities but quantitative differences with respect to the dependence of temporal variability on potential evaporation and precipitation. The main differences occur when the value of E_p/P_{cp} is less than one. Most of the differences may be understood in terms of the differences in runoff formulation discussed earlier. It has also been shown that the temporal variability of the two schemes seems to be largely dependent on the same two physical parameters-potential evaporation and precipitation. These basic similarities lead us to speculate that the physical mechanisms governing soil wetness temporal variability, as well as the form of that dependence, may not be peculiar to the GFDL soil wetness parameterization, but could be of wider relevance.

REFERENCES

Budyko, M., 1974: *Climate and Life.* Academic Press, 508 pp.

Eagleson, P. S., 1978: Climate, soil, and vegetation, Parts 1-7. *Water Resour. Res.*, **14,** 705-776.

Folland, C. K., T. N. Palmer and D. E. Parker, 1986: Sahel rainfall and worldwide sea temperatures, 1901-85. *Nature,* **320,** 602.

Frankignoul, C., and K. Hasselmann, 1977: Stochastic climate models. Part II, Application to sea-surface temperature anomalies and thermocline variability, *Tellus,* **29,** 289-305.

Gordon, H. B., and B. G. Hunt, 1987: Interannual variability of the simulated hydrology in a climatic model—implications for drought. *Climate Dynamics,* **1,** 113-130.

Hansen, J., G. Russell, D. Rind, P. Stone, A. Lacis, S. Lebediff, R. Ruedy and L. Travis, 1983: Efficient three-dimensional global models for climate studies: Models I and II. *Mon. Wea. Rev.,* **111,** 609-662.

Hasselmann, K., 1976: Stochastic climate models. Part I, Theory. *Tellus,* **28,** 473-485.

Jaeger, L., 1976: Monthly Precipitation maps for the entire earth (in German), *Ber. Dtsch. Wetterdienstes,* **18**(139), 38 pp.

Johnson, N. L., and S. Kotz, 1970: *Distributions in Statistics: Continuous Univariate Distributions, Vol. 1.* Wiley, 300 pp.

Jones, R. H., 1975: Estimating the variance of time averages. *J. Appl. Meteor.,* **14,** 159-163.

Katz, R. W., 1977: Precipitation as a chain-dependent process. *J. Appl. Meteor.,* **16,** 671-676.

Kurihara, Y., and J. L. Holloway, Jr., 1967: Numerical integration of a nine-level global primitive equations model formulated by the box method. *Mon. Wea. Rev.* **95,** 509-530.

Lvovitch, M. I., and S. P. Ovtchinnikov, 1964: *Physical-Geographical Atlas of the World* (in Russian). Acad. of Sciences, U.S.S.R., and Department of Geodesy and Cartography, State Geodetic Committee, Moscow (see p. 61).

Manabe, S., and D. G. Hahn, 1981: Simulation of atmospheric variability. *Mon. Wea. Rev.,* **109,** 2260-2286.

——, J. Smagorinsky and R. J. Strickler, 1965: Simulated climatology of a general circulation model with a hydrological cycle. *Mon. Wea. Rev.,* **93,** 769-798.

——, D. G. Hahn and J. L. Holloway, Jr., 1979: Climate simulations with GFDL spectral models of the atmosphere: effect of spectral truncation. *Rep. of the JOC Study Conf. on Climate Models: Performance, Intercomparison and Sensitivity Studies,* Washington, DC, 3-7 April, 1978. GARP Publ. Ser. No. 22, Vol. 1, 41-94. [NTIS N8027917].

Namias, J., 1958: Persistence of mid-tropospheric circulations between adjacent months and seasons. *Rossby Memorial Volume,* Rockefeller Institute Press and Oxford University Press, 240-248.

——, 1963: Surface-atmosphere interactions as fundamental causes of droughts and other climatic fluctuations. *Arid Zone Research,* Vol. 20, *Changes of Climate Proc. of Rome Symp.,* UNESCO, 75700 Paris, France, 345-359.

Orszag, S. A., 1970: Transform method for calculating vector-coupled sums: Application to the spectral form of the vorticity equation. *J. Atmos. Sci.,* **27,** 890-895.

Reynolds, R. W., 1978: Sea surface temperature anomalies in the North Pacific Ocean. *Tellus,* **30,** 97-103.

Rind, D., 1982: The influence of ground moisture conditions in North America on summer climate as modeled in the GISS GCM. *Mon. Wea. Rev.,* **110,** 1487-1494.

Rowntree, P. R., and J. R. Bolton, 1983: Simulation of the atmospheric response to soil moisture anomalies over Europe. *Quart. J. Roy. Meteor. Soc.,* **109,** 501-526.

Shukla, J., and Y. Mintz, 1982: The influence of land-surface evapotranspiration on Earth's climate. *Science,* **215,** 1498-1501.

Walker, J. M., and P. R. Rowntree, 1977: The effect of soil moisture on circulation and rainfall in a tropical model. *Quart. J. R. Meteor. Soc.,* **103,** 29-46.

Yeh, T.-C., R. T. Wetherald and S. Manabe, 1984: The effect of soil moisture on the short-term climate and hydrology change—a numerical experiment. *Mon. Wea. Rev.,* **112,** 474-490.